# Analysis of the Heat Budget of Standard, Cool and Watered Pavements Under Lab Heat-Wave Conditions

Sophie Parison, Martin Hendel, Arnaud Grados, Laurent Royon

# Analysis of the Heat Budget of Standard, Cool and Watered Pavements Under Lab Heat-Wave Conditions

Sophie PARISON[1,2], Martin HENDEL[1,3], Arnaud GRADOS[4], Laurent ROYON[1]

[1] Université de Paris, CNRS, LIED, UMR 8236, F-75006, Paris, France
[2] Paris City Hall, Water and Sanitation & Road and Transportation Departments, Paris, France
[3] Université Gustave Eiffel, ESIEE Paris, département SEN, F-93162 Noisy-le-Grand, France
[4] Université de Paris, MSC, UMR 7057, CNRS, F-75013, Paris, France

## Abstract

The thermal behavior of 12 standard and cool pavement structures (asphalt, granite, stabilized sand, cobblestones, reflective paints, pervious concretes, dry grass, etc.) coupled with pavement-watering is studied in the lab under heat-wave-like conditions. Watering is fine-tuned for each structure to maximize cooling and minimize water consumption using two linear cooling regimes, before deployment in the field. The surface heat budget is closely studied and the partitioning of irradiance and net radiation into conductive, convective, radiative and cooling flux at surface is analyzed for each structure. Energy partitioning, surface temperature increase and optimal watering rates all exhibit good correlation with overall surface absorptivity. The transmitted flux at varying depths is also characterized using a transmission index that includes surface absorptivity and apparent conductivity of the traversed layers. Results of this study intend to improve our understanding of the energy balance of cool pavements compared to traditional ones under given weather conditions, as well as that of processes involved in the optimization of their evaporative cooling versus watering rate. Benefits of each pavement, efficiency of the method, limitations of the protocol and its potential transposition to the field are all discussed in this contribution.

**Keywords:** Cool pavements, Pavement-watering, Evaporative cooling, Surface heat budget, Energy partitioning, Urban heat island, Climate change adaptation, Heat mitigation.

## Highlights

- The thermal behaviour of twelve pavements under heat-wave-like conditions is studied in the lab.
- Pavement-watering is fine-tuned for each structure and the optimal watering rate is determined.
- Partitioning of irradiance and net radiation is calculated using surface heat budgets.
- Good correlation of surface temperature increase and surface energy partitioning fluxes is found with an absorptivity index, and with in-depth heat flux for a transmission index.
- Implications and limitations of this work and its transposition to the field are discussed.

## Nomenclature and Abbreviations

| | |
|---|---|
| $\alpha$ | albedo [-] |
| $a$ | absorptivity index [-] |
| $\varepsilon$ | emissivity [-] |
| e | layer thickness [m] |
| $h$ | convective heat transfer coefficient [W/(m².K)] |
| $H$ | upwards atmospheric convective flux [W/m²] |
| IR | infrared |
| $k$ | apparent thermal conductivity [W/(m.K)] |
| $L$ | incident longwave radiation [W/m²] |
| $L_{up}$ | upwards longwave radiation [W/m²] |
| LW | longwave (3 - 100 µm) |
| NIR | near infrared |
| $\Phi$ | pavement cooling flux [W/m²] |
| *PPCC* | Pervious Portland-cement concrete |
| $Q$ | watering rate [mm/h] |
| $R_n$ | downwards net radiation (total) [W/m²] |
| $S$ | incident shortwave radiation [W/m²] |
| $S_{up}$ | reflected shortwave radiation [W/m²] |
| SW | shortwave (0.3 -3 µm) |
| $S+L$ | irradiance (total) [W/m²] |
| $\sigma$ | Stefan-Boltzmann constant [W/(m².K⁴)] |
| $\tau_i$ | transmission index [-] |
| $T_a$ | air temperature [°C] |
| $T_s$ | surface temperature [°C] |
| $T_z$ | pavement temperature at depth $z$ [°C] |
| UHI | urban heat island |
| $V_z$ | downwards conductive heat flux at depth $z$ [W/m²] |

# 1 Introduction

Major public-health threats posed by heat-waves combined with the urban heat island (UHI) phenomenon have pushed cities to seek out urban cooling and adaptation techniques. This is accelerated by climate change, which predicts an increase in the frequency, duration and intensity of these events (Robine *et al.* 2008, Dousset *et al.* 2011, Meehl & Tebaldi 2004, Lemonsu *et al.* 2013). Depending on the greenhouse gas emission scenario, some parts of the globe are even threatened to become uninhabitable for at least part of the year, with unprecedented challenges for human thermoregulation (Mora *et al.* 2017, Kang & Eltahir 2018, Sherwood & Huber 2010, Hanna & Tait 2015).

As a result, a growing interest from decision-makers and a stimulated research effort are observed regarding urban cooling techniques. A large number of studies – either *in situ*, in the laboratory or numerically simulated – aim to quantify the performance of such methods.

The many benefits of urban greening have been widely studied, either through the planting of trees, developing of green roofs or façades, or creation of parks (De Munck *et al.* 2018, Bowler *et al.* 2010, Chun & Guldmann 2018). Energy efficiency is also important, i.e. aiming to limit the impact of air conditioning during summer (Tremeac *et al.* 2012, De Munck *et al.* 2013) or favoring the use of urban water networks for emergency cooling (Guo & Hendel 2018). Cooling solutions also include so-called "cool materials" (façades, rooftops or pavements), which include reflective, emissive, heat-harvesting, permeable or PCM materials (Santamouris 2013, Santamouris 2015).

Other methods also exist, such as pavement-watering (Hendel *et al.* 2016, Kinouchi & Kanda 1997, Takahashi *et al.* 2010, Yamagata *et al.* 2008, Azam *et al.* 2018), implemented for instance by the City of Paris since 2013 through experimental summer campaigns using the supply of the city's non-potable water network. The method was found to reduce the UTCI-equivalent temperature at pedestrian height up to 3°C during the day despite the increase in relative humidity up to a few percent (Hendel *et al.* 2016, Parison *et al.* 2020a). The study further highlighted the influence of the type of material being watered on the performance of the process.

Although a considerable number of studies address the study of traditional or cool pavements (Qin 2015), some of them providing detailed surface heat budgets (Qin & Hiller 2014, Takebayashi & Moriyama 2012, Anandakumar 1999, Camuffo & Bernardi 1982), the scientific literature suggests this topic should be further examined regarding cool pavements' energy partition and their comparison to traditional ones (Qin 2015). Besides, literature globally lacks comparisons under fixed weather conditions between pavements and studies, namely due to the variability of outdoor conditions, study locations and test protocols. One way of tackling this limitation is to use a lab approach or an *in situ* observation site with various paving structures exposed to the same simultaneous conditions (Takebayashi & Moriyama 2012, Li *et al.* 2013a, Asaeda *et al.* 1996). Several lab studies focusing on the behaviour of pavements with heat-up and cool-down phases were found (Wu *et al.* 2018, Chen *et al.* 2009), some of which include pavement-watering or grass (Ueno & Tamaoki 2009, Shin *et al.* 2019), but to the best of our knowledge these tend to focus on traditional asphalt or Portland-cement concrete pavements. Besides, studies rarely take into account the underlying layers composing realistic pavements and often use a limited number of indicators (i.e. principally temperature), thus setting aside pavement heat budgets, with exceptions (Takebayashi & Moriyama 2012, Qin & Hiller 2014, Li *et al.* 2013b). Finally, we are unaware of any studies attempting to fine-tune pavement-watering for different pavement structures.

Previous work by the authors has addressed these aspects by developing a lab experiment for studying various paving materials under heat-wave like conditions including a day phase with artificial insolation and a night phase, with or without fine-tuning of surface watering (Hendel *et al.* 2018, Parison *et al.* 2020b).

Building on this, the present contribution uses this experimental setup to study the thermo-climatic behaviour, with and without pavement-watering, of a range of Parisian pavement structures, including both conventional (asphalt road and sidewalk, granite sidewalk, cobblestones etc.) and "innovative" structures, which fall under the category of cool pavements (permeable structures, slag concrete, reflective pavements etc.). This work proposes the study of a wide range of road materials under identical weather conditions, allowing for direct comparisons between structures. Given the conditions imposed for the climate cycle, the set-up is not intended to faithfully reproduce outdoor conditions, but is rather used as a comparison tool of the thermal behaviour of various paving structures undergoing the same conditions, though they may differ from a real environment.

Study goals include the analysis and comparison of the behaviour of non-watered Parisian pavements and the optimization of their surface watering via the maximization of the cooling flux jointly with the minimization of the watering rate on the other hand. The relevant parameters (albedo, absorptivity, etc.) that condition the optimal watering rate and the efficiency of the method are highlighted for the paving structures. Lastly, the surface heat budget and energy partition at the pavements' surface is determined and detailed. Through the calculation of the surface heat budget under steady-state conditions, energy partitioning into heat conduction, atmospheric convection and visible/infrared radiosity is thus characterized and detailed for each pavement as a function of a radiation absorptivity index, for dry as well as optimally-watered pavements.

# 2 Methodology

## 2.1 Protocol

The protocol aims to create simplified heat-wave-like conditions typically observed in Paris. Cylindrical pavement samples undergo a 24-hour cycle inside a closed climate chamber including an 8-hour day phase with artificial insolation provided by a halogen lamp, and a 16-hour night phase without insolation. A diagram and photograph of the experimental set-up is provided in Figure 1. The bottom and periphery of the pavement sample are thermally insulated with 5-cm-thick polyurethane foam (thermal conductivity of 0.03 $W.m^{-1}.K^{-1}$) to create a zero heat-flux boundary condition.

During the day, the temperature is set to 35°C with 35% relative humidity, while at night the temperature is 25°C with 70% humidity. These setpoints correspond to conditions typically encountered during heat-waves in Paris as seen in the field with continuous measurements conducted since 2013 (Hendel *et al.*, 2016). Before each trial, samples are stabilized under night phase conditions. The presence of a pressurized-water sprinkler allows surface watering at a selected frequency during the day. Table 1 sums up the characteristics of each phase. The radiation intensity is specified for both short (SW) and long wavelength radiations (LW), respectively of 0.3-3 µm and 3-100 µm. The SW/LW proportion (resp. 70/30%) is measured using a pyrgeometer for the LW band and using a pyranometer with thermopile for the SW band. Irradiance measurements were conducted inside the closed chamber during the day and night phases, and thus take into account SW and LW reflexion within the chamber. Pavement sample thermal behaviour is monitored at a frequency of 0.1 Hz using the surface and in-depth sensors, while air temperature is measured with a thermocouple placed above the sample's surface.

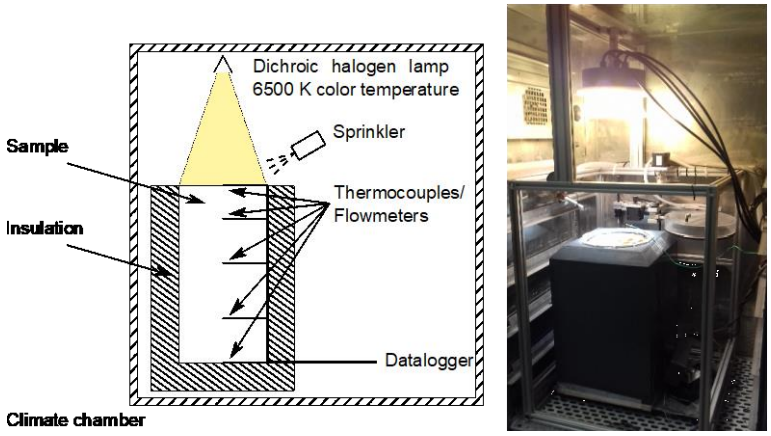


Figure 1: Experimental set-up diagram (left, Hendel *et al.* (2018)) and photograph (right).

Table 1: Characteristics of day and night phases undergoing inside the climate chamber.

| Characteristics | Day phase | Night phase |
|---|---|---|
| Duration | 8 h | 16 h |
| Air temperature | 35°C | 25°C |
| Relative humidity | 35% | 70% |
| SW radiation (0.3-3 µm) | 930 W/m² | 0 W/m² |

| | | |
|---|---|---|
| LW radiation (3-100 µm) | 450 W/m² | 450 W/m² |

Irradiance at the sample surface summarized in Table 1 is of the same order as that of a mid-latitude city under clear summertime skies and low wind speeds (Oke, 1988 & 1997).

## 2.2 Pavement structures

A wide range of tests were conducted in the lab on a total of twelve different pavement structures. Each sample is 32 cm tall and 16 cm in diameter. Half of them are standard pavement structures commonly found in the Parisian urban fabric: asphalt road, asphalt sidewalk, granite sidewalk, stabilized sand, cobblestones and grass. The other half are alternative "innovative" solutions to existing structures: two different reflective paints applied on the traditional asphalt sidewalk, two formulations of pervious Portland-cement concretes (PPCC) sidewalks, a slag concrete sidewalk and a pervious asphalt surface course. Each structure is designed to the specifications of the Paris City Hall except for the two 10 cm-thick PPCC sidewalks which were laid on top of loose sand. An illustration of the different structures' composition is provided in Figure 2.

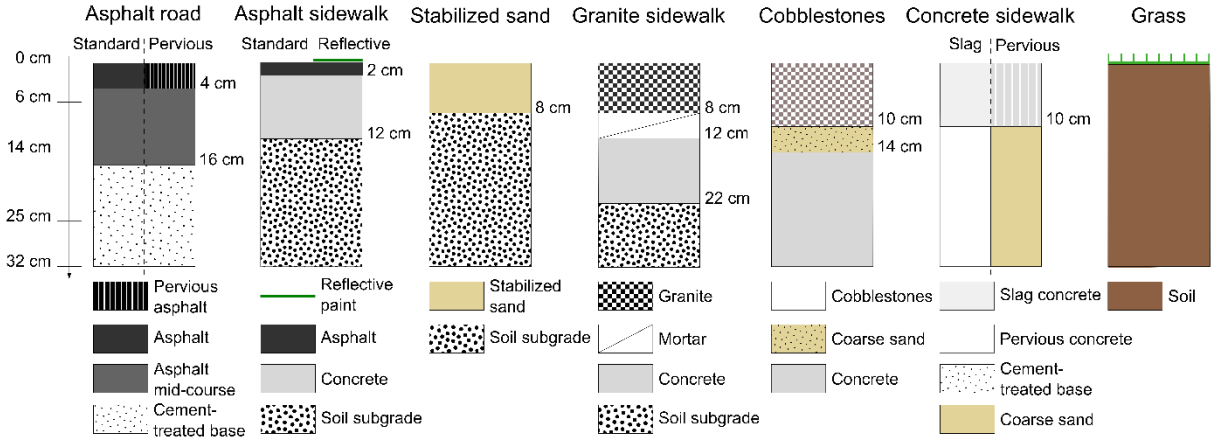


Figure 2: Pavement structures studied in the lab.

All the pervious samples studied, i.e. PPCC 1 and 2 as well as the pervious asphalt, have a porosity of about 15%. In addition, the second PPCC sample incorporates about 20% of expanded clay pebbles in order to improve its water retention ability. Slag concrete incorporates a large proportion of slag cement substituting about 80% of Portland cement, making it more reflective and thermally insulating than traditional Portland-cement concrete. The first reflective paint applied on the asphalt sidewalk is a thermochromic paint which is dark-green at ambient temperature and becomes more reflective in the visible band as it whitens above its transition temperature of 29°C. The second is a near-infrared (NIR) reflective paint, a "cool black". Unlike other structures, paints are a relatively cheap and easy-to-implement option, provided their durability is known (Xie *et al.* 2019). Both paints were mixed with an acrylic binder. A photograph of some samples surfaces is provided in Figure 3.

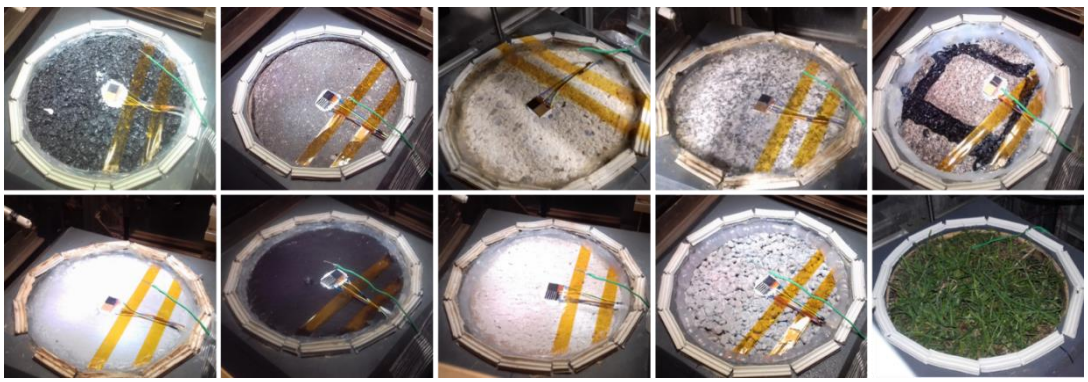

Figure 3: Photograph of some of the tested samples. From left to right and top to bottom: asphalt road, asphalt sidewalk, stabilized sand, granite sidewalk, cobblestones, thermochromic paint (>29°C), NIR reflective paint, slag concrete, PPCC sidewalk 1 and grass.

At the surface, all structures were equipped with a radiative and a black-painted thermo-flowmeter, measuring both heat-flux as well as temperature. Other sensors were placed 6 cm, 14 cm and 25 cm deep,

their nature depending on the samples' composition. Specific subsurface instrumentation is listed in Table **2**. The grass sample was only equipped with thermocouples. Typical uncertainty of the thermocouples (type T) is 0.5°C.

Table 2: In-depth position of the thermal sensors for each structure.

| Instrument | Asphalt road | Pervious asphalt road | Asphalt sidewalk | Stabilized sand | Granite sidewalk | Cobble-stones | Slag concrete sidewalk | PPCC sidewalks |
|---|---|---|---|---|---|---|---|---|
| Thermo-flowmeter | 6 cm<br>14 cm | 6 cm<br>14 cm | 6 cm | 6 cm | 6 cm<br>14 cm | 11 cm | 6 cm<br>14 cm | 10 cm<br>14 cm |
| Type-T thermocouple | 25 cm | 25 cm | 14 cm<br>25 cm | 14 cm<br>25 cm | 25 cm | 14 cm<br>25 cm | 25 cm | 25 cm |

The spectral reflectance of each sample surface was measured following the ASTM E903 standard with a UV-Vis-NIR Cary 5000 spectrophotometer and 150 mm integrating sphere (ASTM, 2012). To obtain a result representative of the entire surface for heterogeneous structures, a minimum of five measurements were made at different positions. In each case, the relative measurement uncertainty is between 1% and 5% depending on the sample. Figure 4 illustrates the resulting averaged spectral reflectivity of the dry pavement structures. In addition to dry surfaces, the spectral reflectance of the moist samples was also measured following ASTM E903. For this procedure, the samples were completely soaked with water prior to conducting the standard ASTM E903 measurement. For the thermochromic asphalt, two sets of measurements were performed independently: one at ambient temperature (<29°C), and another preheating the sample inside a climate chamber set to 50°C in order for the paint to turn reflective (>29°C).

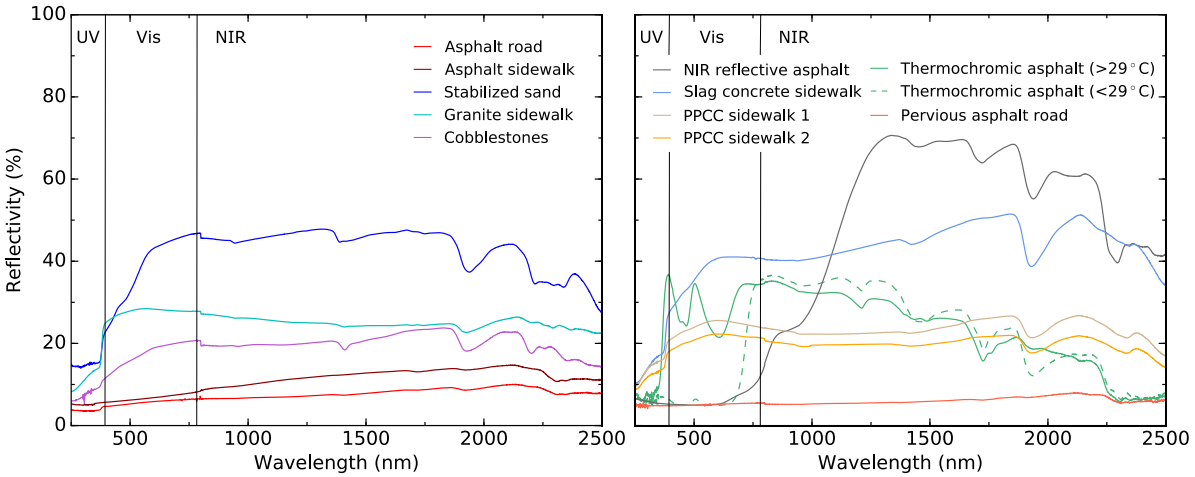


Figure 4: Spectral reflectance averaged over several trials for each dry pavement structure.

Spectral reflectance was weighted using the irradiance spectrum of the halogen lamps to determine the effective albedo of the samples under the experimental conditions (Hendel *et al.* 2018). Surface emissivity was also measured using the reference black body method with a FLIR B400 infrared (IR) camera with a spectral band of 7.5 - 13 µm using black tape with a known emissivity of 0.95.

The albedo of each structure, both dry and wet, as well as emissivity values, are summarized in Table 3. For comparison, AM 1.5 albedo is also provided. Albedo with both spectra differ for surfaces for which a significant difference of reflectivity is observed between the visible and near-infrared bands. Of interest, the albedo of the NIR reflective paint marginally increases when wet.

Table 3: Albedo and emissivity of the studied paving structures.

| Structure surface | Albedo Halogen spectrum | | Albedo Solar spectrum AM 1.5 | | Emissivity |
|---|---|---|---|---|---|
| | dry | wet | dry | wet | dry |
| Asphalt road | 0.076 | 0.057 | 0.070 | 0.055 | 0.99 |
| Asphalt sidewalk | 0.094 | 0.058 | 0.081 | 0.050 | 0.98 |
| Stabilized sand | 0.438 | 0.387 | 0.396 | 0.323 | 0.92 |
| Granite sidewalk | 0.264 | 0.221 | 0.260 | 0.222 | 0.99 |
| Cobblestones | 0.192 | 0.144 | 0.178 | 0.132 | 0.99 |
| Thermochromic paint (>29°C) | 0.308 | 0.266 | 0.292 | 0.258 | 0.97 |
| NIR reflective paint | 0.303 | 0.310 | 0.193 | 0.201 | 0.95 |
| Slag concrete sidewalk | 0.409 | 0.308 | 0.380 | 0.281 | 0.98 |
| PPCC sidewalk 1 (w/o clay pebbles) | 0.233 | 0.130 | 0.232 | 0.124 | 0.97 |
| PPCC sidewalk 2 (w/ clay pebbles) | 0.203 | 0.111 | 0.202 | 0.104 | 0.97 |
| Pervious asphalt road | 0.063 | 0.048 | 0.054 | 0.040 | 0.98 |

The apparent thermal conductivity of the upper layers was determined using Fourier's law under semi steady-state conditions reached at the end of the day phase. Obtained values are summarized in Table 4. The conductivity $k_i$ of the layer $i$ between depths $z_i$ and $z_{i-1}$ is thus obtained using corresponding depths temperature T and heat-flux measurements as follows, as described by Hendel *et al.* (2018):

$$V_{z_i} = V_{z_{i-1}} = \frac{k_i}{z_{i-1} - z_i} (T_{z_{i-1}} - T_{z_i}) \quad (1)$$

Table 4: Apparent thermal conductivity k ($W.m^{-1}.K^{-1}$) of pavement structures' upper layers.

| Layer | Asphalt road | Asphalt sidewalk | Stabilized sand | Granite sidewalk | Cobble-stones | Slag concrete sidewalk | PPCC sidewalks | Pervious asphalt road |
|---|---|---|---|---|---|---|---|---|
| 0-6 cm | 0.88 | 0.69 | 0.35 | 1.16 | 0.85 (0-11 cm) | 0.28 | 0.73 (0-10 cm) | 0.86 |
| 6-14 cm | 2.03 | 1.52 | 0.64 | 1.49 | 0.35 (11-14 cm) | 0.45 | 0.35 (10-14 cm) | 2.03 |

## 2.3 Surface heat budget

The methodology described hereafter is thoroughly developed in previous publications (Hendel *et al.* 2015, Parison *et al.* 2020b).

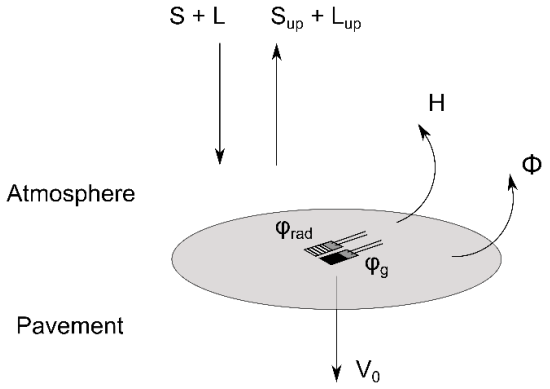


Figure 5: Heat budget of a pavement surface. Flows measured by a radiative heat flow sensor and a global fluxmeter (both sensors with $\varepsilon$=0.95, $\alpha$=0.05) are denoted $\varphi_{rad}$ and $\varphi_g$ respectively.

The surface heat budget of the pavement surface is illustrated in Figure 5. For a dry surface, it is completely described by equation (2):

$$R_n^{dry} = H^{dry} + V_0^{dry} \quad (2)$$

with $R_n$ the net downward radiation received by the surface, $H$ the upward atmospheric convective heat flux and $V_0$ the downward conduction heat flux at the surface. If the surface undergoes pavement-watering, the budget is:

$$R_n^{wet} = H^{wet} + V_0^{wet} + \Phi \quad (3)$$

with $\Phi$ the total cooling flux due to watering. $\Phi$ includes a sensible and a latent cooling component. The former is provided as the sprinkled water heats up, the latter as the sprayed water film evaporates:

$$\Phi = lE + c_p \rho Q (T_s^{wet} - T_w) \quad (4)$$

with $l$ the latent heat of vaporization of water (2,260 kJ/kg); $E$ the evaporation rate; $c_p$ the specific heat of water (4.18 kJ.kg$^{-1}$.K$^{-1}$); $\rho$ its density (1,000 kg.m$^{-3}$); $Q$ the watering rate; $T_s^{wet}$ the surface temperature when wet; and $T_w$ the water temperature (35°C during the day phase). Experimentally, $\Phi$ is obtained by subtracting equation (3) from equation (2):

$$\Phi = \Delta H^{dry-wet} + \Delta V_0^{dry-wet} - \Delta R_n^{dry-wet} \quad (5)$$

The convective and radiative terms, $\Delta H^{dry\text{-}wet}$ and $\Delta R_n^{dry\text{-}wet}$ respectively, are determined using the respective definitions for the atmospheric convective heat flux and net radiation, detailed in the following equations and applied to data from dry and watered trials of the same sample:

$$H = h(T_s - T_a) \quad (6)$$

$$R_n = (1 - \alpha)S + \varepsilon(L - \sigma T_s^4) \quad (7)$$

Hence, since air temperature $T_a$ and incident irradiance received at sample surface ($S$+$L$) do not vary between trials:

$$\Delta H^{dry-wet} = h^{dry} T_s^{dry} - h^{wet} T_s^{wet} - (h^{dry} - h^{wet}) T_a \quad (8)$$

$$\Delta R_n^{dry-wet} = \sigma\left(\varepsilon_{wet} T_s^{wet\,4} - \varepsilon_{dry} T_s^{dry\,4}\right) + \left(\varepsilon_{dry} - \varepsilon_{wet}\right) L + (\alpha_{wet} - \alpha_{dry}) S \quad (9)$$

with $h^{dry}$ *and* $h^{wet}$ the respective convective heat transfer coefficient for a dry and wet surface, $T_s$ the surface temperature, α albedo, $\varepsilon$ emissivity, $S$ and $L$ respectively short and longwave radiations and $\sigma$ the Stefan-Boltzmann constant. Assuming that the difference between the convective exchanges coefficients for dry and watered trials is negligible (i.e. $h = h^{dry} \approx h^{wet}$), equation (8) then becomes:

$$\Delta H^{dry-wet} = h(T_s^{dry} - T_s^{wet}) \quad (10)$$

This hypothesis was validated by comparing the mean evaporation rate for each trial calculated using two methods: the surface heat budget on the one hand and the mass convection transport problem (based on the water vapour pressure gradient in near air) on the other hand (see Parison *et al.* 2020). Results using these two methods converge for a difference less than 3 W/m²/K between $h^{dry}$ *and* $h^{wet}$. For the rest of this paper, a single convective coefficient noted $h$ is thus considered for all trials.

Finally, $V_0^{dry}$ is estimated as a residual of the surface energy balance, while the conduction term, $\Delta V_0^{dry\text{-}wet}$, is obtained experimentally by using the difference between the fluxes measured by the sensors 6 cm deep, between a dry and a watered test. This assumes that the thermal properties of the samples are not influenced by watering and that the flow absorbed by the first 6 centimetres is constant regardless of the test. This hypothesis has been found to be experimentally validated in previous work (Parison *et al.* 2020b).

The estimation of these different parameters therefore allows us to calculate the maximum cooling flux $\Phi$ for each watering rate and sample.

## 2.4 Optimization goals

The present research aims to optimize the effects of watering on different pavements on the basis of a framework previously developed by Hendel *et al.* (2015). The goal of pavement-watering in this study is to decrease the pavement surface temperature, which in turn limits atmospheric heating and helps improve pedestrian thermal stress. As only thermal measurements are performed inside the climate chamber, the following optimization goals are selected:

- Maximise the pavement cooling flux, $\Phi$
- Minimize the watering rate, $Q$

These goals can be combined into maximizing the ratio of pavement cooling to watering rate, $\Phi/Q$.

According to equation (4), the total cooling flux $\Phi$ versus $Q$ is expected to be linear with two regimes: latent and sensible. During the latent regime, all the sprinkled water evaporates, with watering cycles separated by periods when the surface is dry. In the sensible regime, evaporation is maximized for a given structure and

the only gain from additional watering comes from the sensible cooling. The latent and sensible regimes are respectively expressed by equation (11) and (12):

$$\Phi_{reg,\ lat} = lQ + c_p \rho Q(T_s^{wet} - T_w) \qquad \text{while } E=Q \tag{11}$$

$$\Phi_{reg,\ sens} = lE^{max} + c_p \rho Q(T_s^{wet} - T_w) \qquad \text{once } Q>E^{max} \tag{12}$$

The intersection of these regimes renders the maximum ratio for $\Phi/Q$. In principle, regardless of the material, in the first regime all the water evaporates. Thus, plotting $\Phi$ versus $Q$, the expected slope for this regime is the latent heat of vaporization of water $l$ (2,260 kJ/kg), i.e. the cooling flux created by evaporating 1 mm of water per hour (630 W/m² per mm/h). Therefore, the optimal watering rate can theoretically be obtained by intersecting the latent regime's 630 W/m²/(mm/h) slope with a zero-slope segment whose intercept is the maximum cooling flux reached during the sensible regime for a high watering rate ($Q>>E^{max}$). This approximation, however, requires neglecting sensible cooling in both regimes, (hence $\Phi_{reg,\ lat} = lQ$ and $\Phi_{reg,\ sens} = lE^{max}$), as illustrated in Figure **6**. In practice, this can be achieved by performing only one highly watered 24-h test to estimate the cooling flux of the sensible regime.

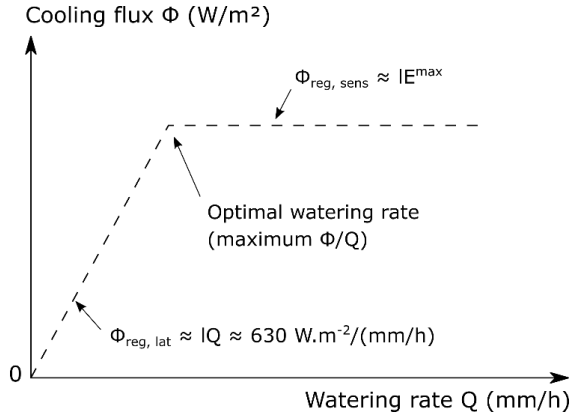


Figure 6: Schematic representation of the so-called latent and sensible cooling regimes when neglecting sensible cooling for each regime.

The first section of results of this paper presents the dry behaviour of the pavements during the entire 24-h trial.

The second focuses on the maximization of $\Phi/Q$ in steady-state, i.e. determining the corresponding optimal watering rates and cooling flux for all the pavements, following the methodology of section 2.3. In order to do so, a wide range of watering rates were implemented to visualize both cooling regimes. Results from this optimization are then compared with the theoretical approach described in the previous paragraph (Figure **6**).

Lastly, having completed this optimization, the third results section presents the steady-state thermal analysis and comparison of the dry and optimally-watered pavements. Energy partitioning, detailed heat-budgets and in-depth heat transmission are examined. In the end, the set-up is used to identify key parameters influencing the optimization of watering.

# 3 Pavements dry behaviour

## 3.1 Surface temperature

We start by briefly presenting the non-watered temperatures of the structures. Surface behaviour of the samples is illustrated in Figure 7. Typical uncertainty on all presented temperature signals is about 0.5°C.

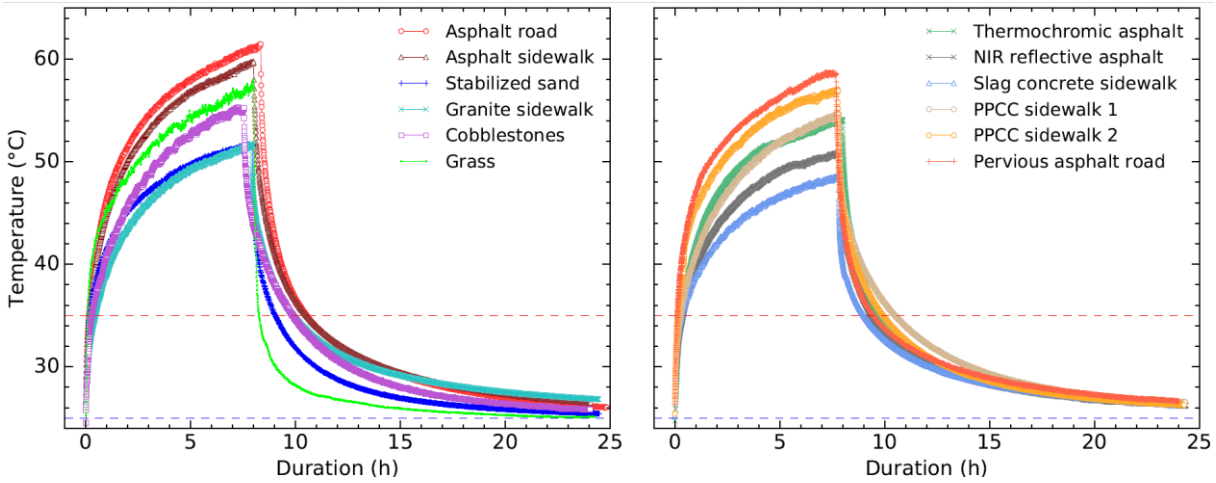


Figure 7: Surface temperatures of standard (left) and innovative (right) pavement structures over a 24-h non-watered trial. Dashed red and blue lines respectively represent day phase (35°C) and night phase (25°C) air temperature setpoints.

The non-watered behaviour of the standard structures (except for cobblestones) and of a grass sample amply watered prior to the experiment has been described in Hendel *et al.* (2018). During the day, an exponential rise of surface temperature is exhibited for all samples, followed by a sudden drop as soon as the lamps are switched off and the air temperature setpoint is changed. With regard to initial work, irradiance of the halogen lamps has been slightly reduced to better match that of *in situ* conditions given the set-up, which only caused a small reduction of end-of-day-phase temperatures (2° to 3.5°C) for the previously tested pavements.

During the night, temperatures decrease towards their setpoint temperature, i.e. 25°C. This appears to be more rapidly achieved for the stabilized sand and the slag concrete sidewalks. At the end of the day phase, the structure with the lowest temperature is the slag concrete sidewalk with 48.4°C.

Contrary to previous work, the grass sample was not watered before the trial. As a result, the grass dried very quickly and turned yellow at the end of the trial. Unable to evapotranspirate, its surface temperature increased almost as high as that of the asphalt sidewalk (~58°C). In contrast, previously amply watered grass maintained a temperature of about 40°C under similar conditions. Similar results are found in the literature, confirming that the cooling efficiency of vegetation and its positive impact on air temperature and pedestrian heat stress strongly relies on its irrigation (Daniel *et al.* 2018).

For the asphalt sidewalk structure, the application of reflective paint leads to a reduction of 5.7° and 8.9°C respectively for the thermochromic and the NIR reflective paints, making it as cool as the most reflective standard pavement tested (stabilized sand). Similar reductions can be found in the literature for green thermochromic and black NIR reflective paints (resp. 8° and 13°C) with comparable albedo (Karlessi *et al.* 2009, Levinson *et al.* 2007).

Surface temperatures seem to be principally driven by albedo, as darker pavements tend to be hotter and brighter ones cooler. Figure 8 illustrates the maximum increase of surface temperature compared to air temperature with a linear regression versus albedo and versus a dimensionless absorptivity index defined as follows:

$$a = \frac{S(1-\alpha) + L\varepsilon}{S+L} \tag{13}$$

The global surface absorptivity of eq. (13) takes into account SW and LW absorptivities, resp. (1-α) and $\varepsilon$, and weights each by the corresponding proportion of SW and LW irradiance, i.e. 70% and 30% resp.

As a can be seen, a reduction of nearly 3°C is obtained per 0.1 increase in albedo. This falls within the lower boundary of the typical range of 3° to 7°C found in the literature for different slabs, pavement and roof tiles (Qin & Hiller 2014, Li *et al.* 2013a, Levinson *et al.* 2007, Synnefa *et al.* 2007, Pomerantz 2000, Pomerantz *et al.* 2003). Although both paints have a very similar albedo (0.308 vs 0.303) and were applied on the same sample, thermochromic asphalt ends up 3.2°C hotter than the NIR reflective asphalt. Beyond the reasonable measurement accuracy (±0.5°C), this can be attributed to differences between fresh paint prior to albedo measurement and its ageing inside the chamber, despite our precautions.

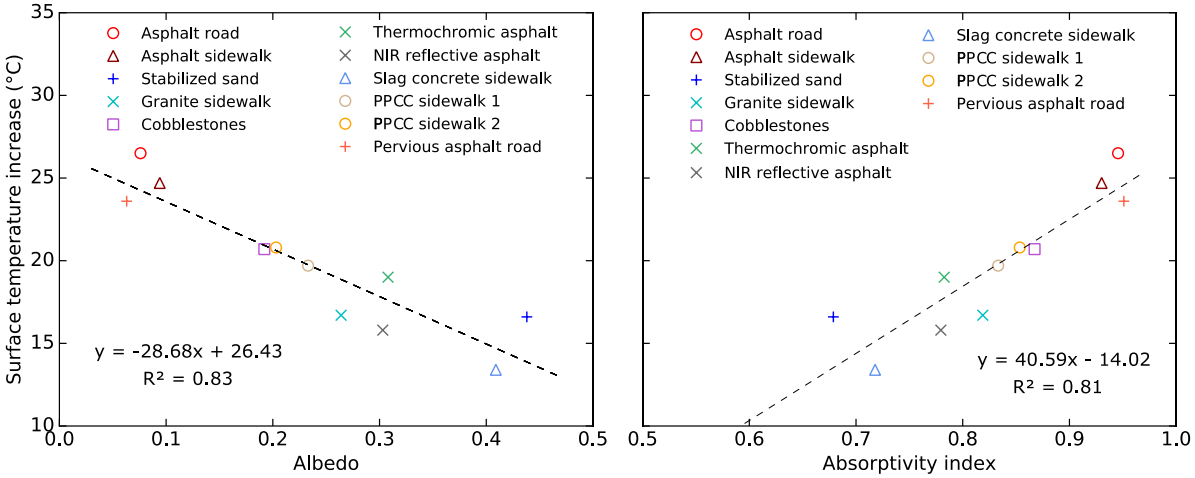


Figure 8: Daily surface temperature increase during a dry test versus albedo (a) and versus the absorptivity index (b).

Finally, Figure 8 predicts negative values of the surface increase temperature, i.e. the existence of materials that would provide radiative cooling even in daytime. In principle, such materials should become colder than the air provided convection is low. Based on the regressions, it would require an albedo of at least 0.91 under the conditions of the lab. This aspect needs further investigation and is briefly discussed in section 7.

## 3.2 In-depth temperature

In-depth temperatures for a dry trial are provided in Figure 9.

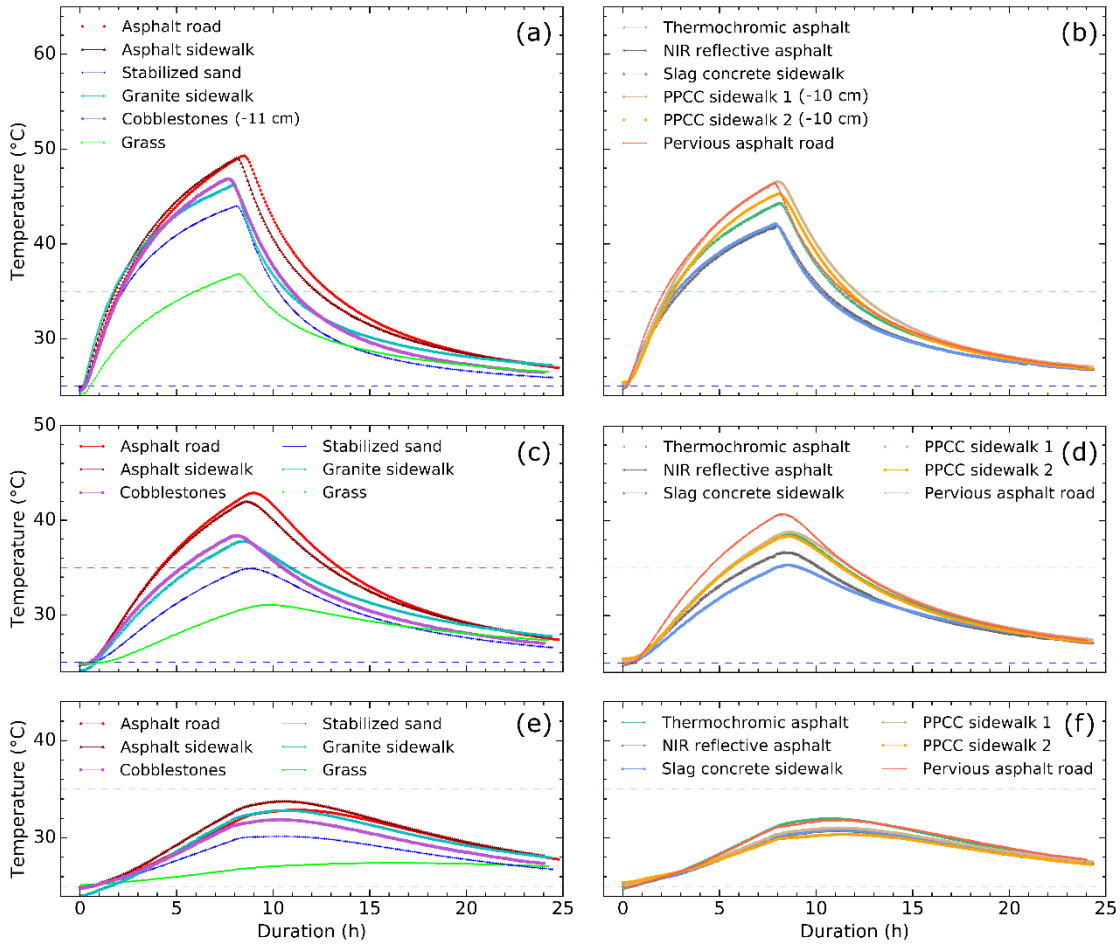


Figure 9: In-depth temperatures of standard (left-hand side) and innovative (right-hand side) dry pavement structures 6 (a and b), 14 (c and d) and 25 (e and f) cm deep. Dashed red and blue lines respectively represent day phase (35°C) and night phase (25°C) air temperature setpoints.

Thermochromic and NIR reflective asphalts remain cooler in-depth compared to the traditional asphalt sidewalk thanks to their higher albedo. Also, although the stabilized sand and the granite sidewalk exhibit similar "cool" behaviours at the surface, the latter stands out in depth by being progressively hotter than stabilized sand, ending up as hot as asphalt road and sidewalk 25 cm deep. This was explained by Hendel *et al.* (2018) as caused by the high effusivity ($\sqrt{k.\rho.c_p}$) and diffusivity ($^{k}/_{\rho c_p}$) of the granite structure (granite, mortar and concrete), causing it to both rapidly absorb heat while limiting surface temperature increase, and quickly transmit the temperature signal to lower depths. As an example, the contrary is observed for the PPCC sidewalks, relatively hot at the surface and as far as 14 cm deep, but remaining cool 25 cm deep due to the low diffusivity of the sand base layer. Although the exact diffusivity of the layers and materials was not measured, information regarding the diffusive capacities of the structures is given looking at the time lag between each in-depth temperature peak with regard to the surface peak.

The grass sample, although relatively hot at the surface, stands out in-depth as it remains significantly cooler than other pavements. Although not measured, we presume this is due to the low thermal conductivity of loose dry soil relatively to the other materials. Since only temperature measurements were performed for the grass, this sample is not discussed further hereafter.

# 4 Optimization of watering

## 4.1 Temperature reductions with watering

We now turn to the analysis of the temperature reductions caused by watering of the pavements. For the asphalt road and sidewalk, the granite sidewalk, the stabilized sand, the thermochromic and NIR reflective asphalt and the slag concrete sidewalk, a total of twelve different watering rates were applied ranging from 0.1 to 3.0 mm/h (equivalent to L/(m².h)). Typical uncertainty on the watering rate is estimated to be about 0.05 mm/h. Having fine-tuned the watering rate for these samples, fewer watering rates (six in total) were applied for the remaining structures, tested afterwards.

When watered, surface temperature amplitude is significantly reduced and presents peaks at a fixed frequency, corresponding to the change from cooling to heating once the water film has dried. For high watering rates, those peaks tend to disappear, meaning that the optimal watering rate has been reached and that the surface no longer dries between two consecutive water sprays (Parison *et al.* 2020b). The optimal watering rate is thus obtained when the time span between two consecutive sprays is equal to the surface drying period. Watered temperature signals are not presented here.

Figure 10 shows the difference in maximum surface temperatures as a function of the watering rate $Q$. For all the upcoming analyses, steady-state (or quasi steady-state) results are shown, corresponding to the end of the 8-h day phase.

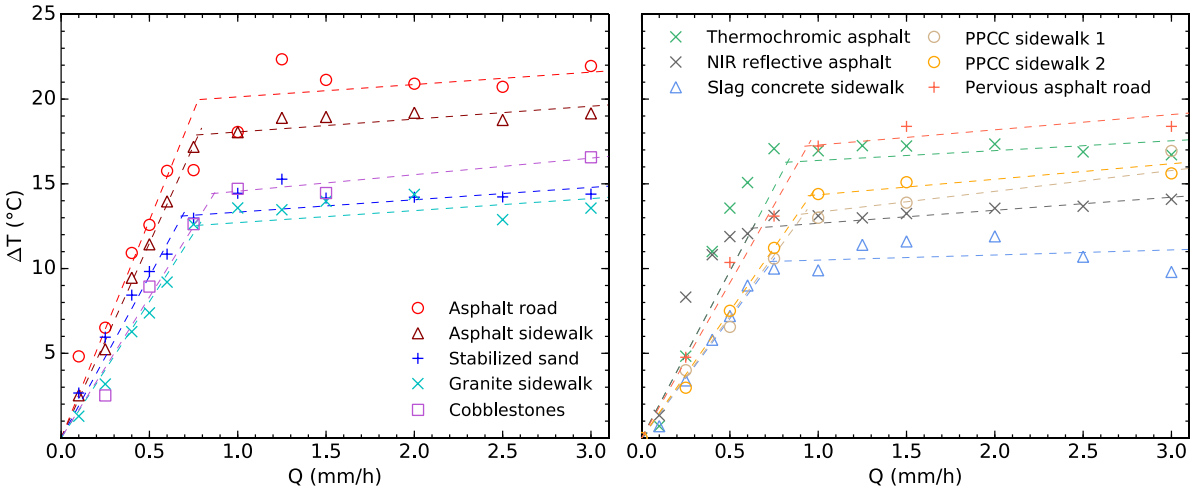


Figure 10: Maximum surface temperature dry-wet difference versus watering rate $Q$ for traditional (left) and innovative pavements (right). The double piecewise linear regression is represented with dashed lines (see Table 5 for regression statistics).

For all pavements, strong surface temperature reductions are exhibited with watering, ranging from 10° to 22°C. Higher decreases are observed for dark structures (asphalt road and sidewalk), as their final dry temperature is greater. With a watering rate of 3 mm/h, the steady-state temperature of each sample converges towards 40°C.

The two linear cooling regimes predicted by equation (4) are observed, corresponding respectively to the increase in evaporation due to watering, then to the marginal increase of cooling once the maximum evaporation rate is reached. A double piecewise linear regression with a forced zero-intercept is used to model these regimes and is represented with dashed lines. In each case, an $R^2$ coefficient greater than 0.80 is found for both regimes. The optimal watering rate $Q_{opti}$ is the intersection of the two segments and maximizes the cooling effects while minimizing the water consumption. Results of the regressions are summarized in Table 5.

Table 5: Best fitting equations for both cooling regimes and corresponding optimal watering rate $Q_{opti}$ for each pavement.

| Pavement structure | Segment 1 | Segment 2 | $Q_{opti}$ (mm/h) |
|---|---|---|---|
| Asphalt road | $y_1 = 25.7\ Q$ | $y_2 = 0.73\ Q + 19.4$ | 0.80 |
| Asphalt sidewalk | $y_1 = 23.0\ Q$ | $y_2 = 0.76\ Q + 17.3$ | 0.78 |
| Stabilized sand | $y_1 = 19.1\ Q$ | $y_2 = 0.73\ Q + 12.6$ | 0.69 |
| Granite sidewalk | $y_1 = 16.1\ Q$ | $y_2 = 0.71\ Q + 12.0$ | 0.78 |
| Cobblestones | $y_1 = 16.6\ Q$ | $y_2 = 0.98\ Q + 13.6$ | 0.86 |
| Thermochromic asphalt | $y_1 = 19.7\ Q$ | $y_2 = 0.58\ Q + 15.8$ | 0.83 |
| NIR reflective asphalt | $y_1 = 19.7\ Q$ | $y_2 = 0.77\ Q + 11.9$ | 0.63 |
| Slag concrete sidewalk | $y_1 = 14.1\ Q$ | $y_2 = 0.30\ Q + 10.2$ | 0.74 |
| Pervious sidewalk 1 (w/o clay) | $y_1 = 14.4\ Q$ | $y_2 = 1.23\ Q + 12.1$ | 0.92 |
| Pervious sidewalk 2 (w/ clay) | $y_1 = 15.0\ Q$ | $y_2 = 0.92\ Q + 13.4$ | 0.96 |
| Pervious asphalt road | $y_1 = 18.3\ Q$ | $y_2 = 0.90\ Q + 16.4$ | 0.94 |

Globally, reflective (thus cooler) structures tend to have a lower optimal watering rate. This is however untrue for the pervious asphalt road and PPCC sidewalks, for which the highest $Q_{opti}$ values are exhibited, most likely because of infiltration of sprinkled water. Very similar observations are made in-depth, although they are not presented here. The amplitude of the temperature reductions in-depth is smaller (with reductions of 7° to 12°C at 6 cm, 3° to 9°C at 14 cm and 0.5° to 3.5°C 25 cm deep), but the ranking of the "most cooled" pavement structures exhibited in Figure 10 is preserved.

## 4.2 Conductive, convective and radiative dry-wet variations

We now analyze the surface heat budget to determine $\Delta V_0^{dry\text{-}wet}$, $\Delta H^{dry\text{-}wet}$ and $\Delta R_n^{dry\text{-}wet}$ (eq. (5)) respectively representing reductions in the conductive and convective heat flows and the increase in net radiation due to watering. These terms are illustrated in Figure 11.

For dry trials, a convective exchange coefficient of about 10 W/(m².K) was found. For watered tests, the emissivity of the water (i.e. 0.98) is systematically assumed. Error bars were obtained by propagating the uncertainties of terms involved in equations (9) and (10) or using the standard deviation of the dry-wet difference between 6 cm deep signals during daytime for $\Delta V_0^{dry\text{-}wet}$.

In Figure 11 (a) and (b), heat storage is found to be greatly reduced by watering, i.e. $\Delta V_0^{dry\text{-}wet}$ increases with $Q$. The structure most impacted by watering is the granite sidewalk, although the latter remains relatively "cool" at its surface due to its high albedo. This is most likely due to its high conductivity. The contrary prevails for stabilized sand, poorly conductive. The same tendency is observed in Figure 11 (b): slag concrete exhibits the lowest reduction due to its very low conductivity.

In Figure 11 (c) and (d), convective exchanges between the surface and the ambient air decrease with $Q$, thus $\Delta H^{dry\text{-}wet}$ gradually increases with watering. This is directly proportional to the surface temperature difference between dry and wet trials, as shows equation (10). Since the convective exchange coefficient $h$ is similar for each structure (~10 W/(m².K)), tendencies follow that of such surface temperature differences shown in Figure 10. Hottest structures are therefore more impacted by watering than cooler ones.

Finally, in Figure 11 (e) and (f), $\Delta R_n^{dry\text{-}wet}$ decreases significantly with $Q$, i.e. net radiation increases with watering. Regarding its value, competing effects are at work. Indeed, low-albedo structures exhibit strong decreases as well as some of the high-albedo pavements, such as slag concrete. Yet, the NIR reflective sidewalk, also highly reflective, exhibits the lowest reduction of all the samples. We thus consider each term

of $\Delta R_n^{dry\text{-}wet}$ separately (see eq. (9)), i.e. the dry-wet reductions of black-body emission $\sigma(\varepsilon_{wet}T_s^{wet\,4} - \varepsilon_{dry}T_s^{dry\,4})$, of reflected infrared radiation $(\varepsilon_{dry} - \varepsilon_{wet})L$, and of reflected visible radiation $(\alpha_{wet} - \alpha_{dry})S$. Those terms are normalized by irradiance $S$+$L$ and illustrated in Figure 12 for each pavement's optimal watering rate (see Table 6 in next section).

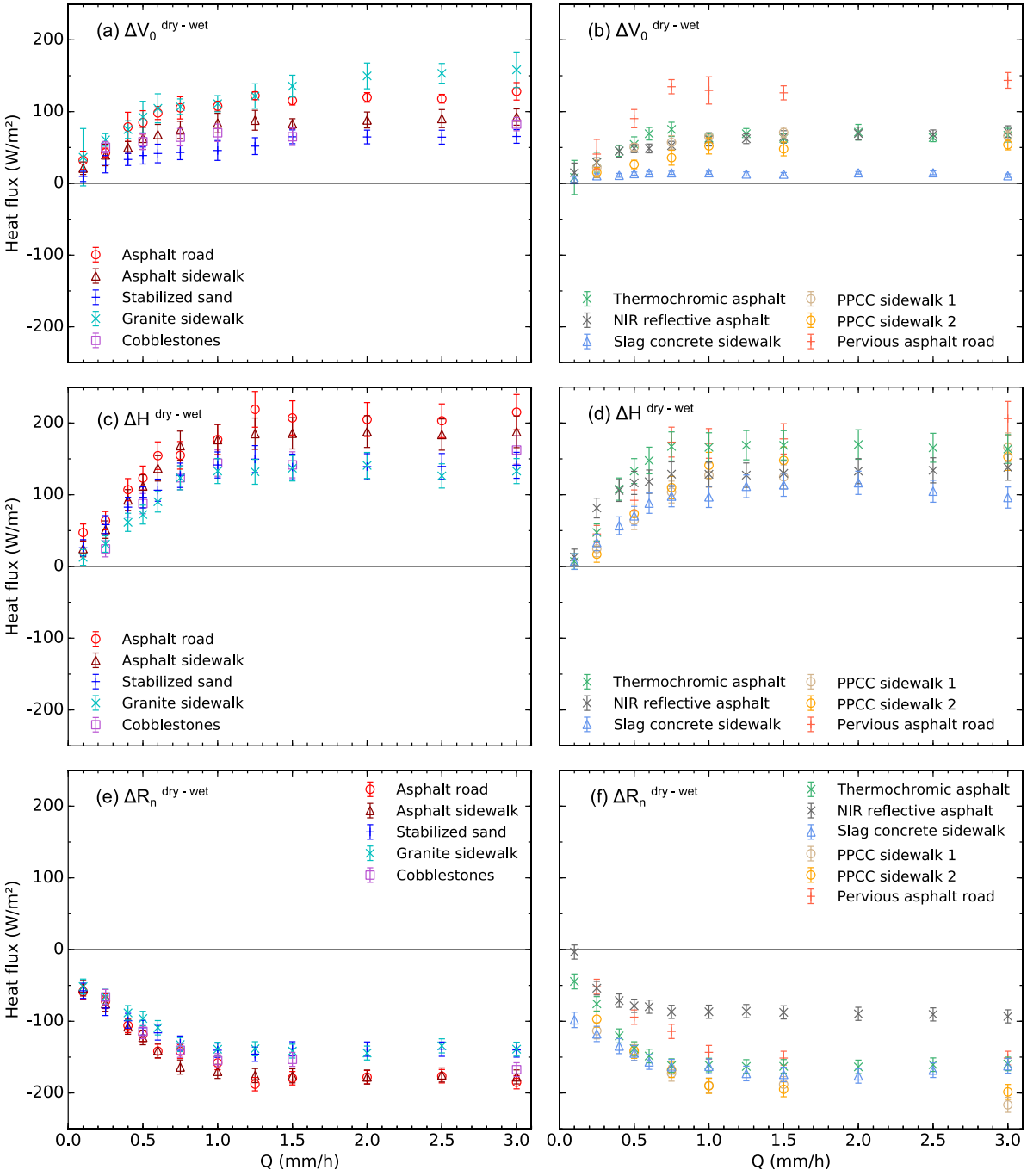


Figure 11: From top to bottom, dry-wet differences of conductive heat flux $\Delta V_0^{dry\text{-}wet}$, net radiation $\Delta R_n^{dry\text{-}wet}$ and convective flux $\Delta H^{dry\text{-}wet}$ as a function of the watering rate $Q$, for standard (left column) and innovative pavements (right column).

As mentioned, structures with high black-body emission reduction are those with important temperature reductions with watering (low-albedo structures). The reduction in reflected infrared radiation is either null or negligible with regard to total net radiation reduction, since pavement emissivities are close to that of water and since LW only represents 30% of the incident irradiance. This term is only positive for the asphalt road, granite sidewalk and cobblestones whose emissivity is higher than that of water. Lastly, pavements with important variations in albedo when watered (about -10%), i.e. PPCC and slag concrete sidewalks,

exhibit a reduction of reflected visible radiation greater than that of their black-body emission, thus offsetting the small temperature difference.

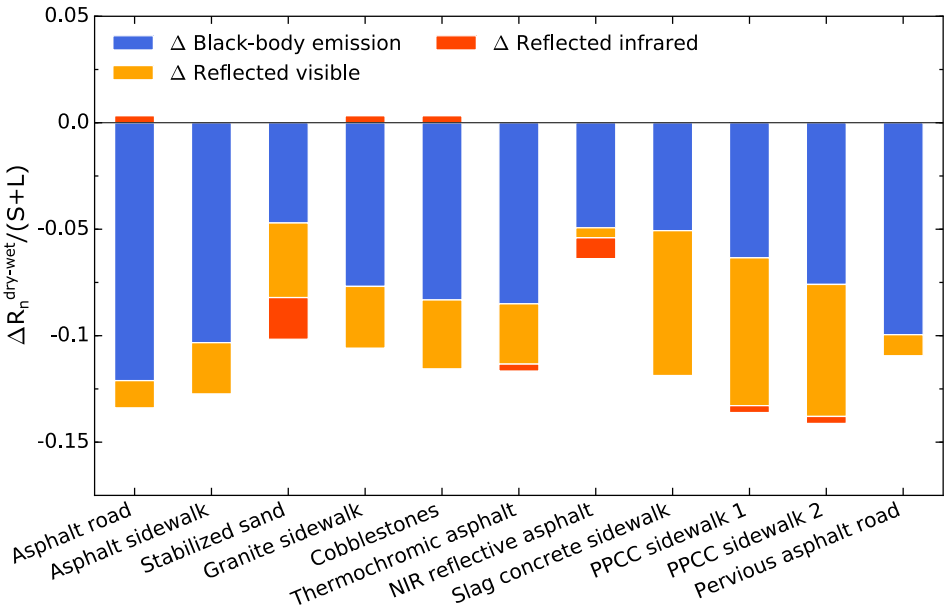


Figure 12: Dry-wet differences in black-body emission, reflected infrared and reflected visible radiation divided by total irradiance for each pavement at their optimal watering rate.

## 4.3 Total pavement cooling flux

Knowing $\Delta V_0^{dry\text{-}wet}$, $\Delta H^{dry\text{-}wet}$ and $\Delta R_n^{dry\text{-}wet}$, it is possible to calculate the total cooling flux $\Phi$ with equation (5) for each watering rate and pavement under steady-state conditions. This is shown in Figure 13. As predicted by equation (4), again, a double piecewise linear regression with forced zero intercept is performed and represented with dashed lines. Uncertainties are propagated for $\Phi$ through equation (5). Results are summarized in Table 6.

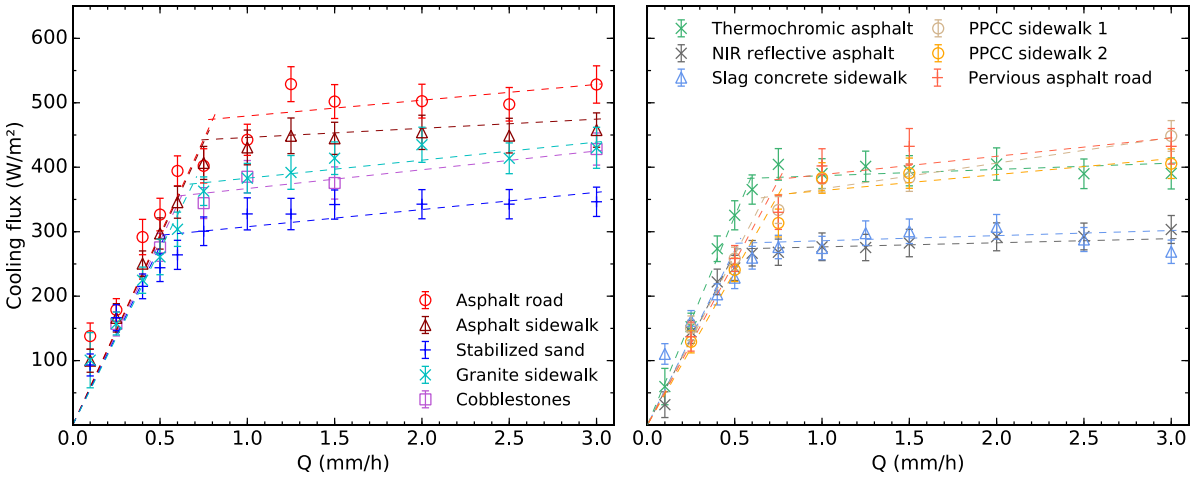


Figure 13: Total cooling flux $\Phi$ as a function of the watering rate $Q$ for traditional structures (left) and alternative pavements (right). The double piecewise linear regression is represented with dashed lines. (see Table 6 for regression statistics).

For the asphalt road, maximum cooling is up to 500 W/m². This is about twice as much as field observations (Hendel *et al.* 2015), most likely because of the amount of daily absorbed net radiation which is also doubled in the lab (Parison *et al.* 2020b). Taking into account that the heat budget is doubled in the present lab study, similar values (200-250 W/m² on average) were found on an amply water water-retaining asphalt (10 mm/h) by Takebayashi & Moriyama (2012).

The amplitude of total cooling versus $Q$ reflects observations of the previous section: main factors influencing the total cooling potential are low albedo (high $\Delta H^{dry\text{-}wet}$ and $-\Delta R_n^{dry\text{-}wet}$), high dry-wet albedo variation $\Delta a$ (high $-\Delta R_n^{dry\text{-}wet}$) and high thermal conductivity $k$ of the surface course (high $\Delta V_0^{dry\text{-}wet}$). As a

result, dark structures tend to be cooled more since they combine at least two out of three of the principal contributing factors to $\Phi$, i.e. $\Delta H^{dry\text{-}wet}$ and $-\Delta R_n^{dry\text{-}wet}$. Potential limiting effects to $\Phi$ thus tend to be of less importance, such as the thermal conductivity or albedo variation, which is typically low if albedo is as well.

Table 6: From left to right: optimal value of $\Phi$, best fitting equations for both regimes, optimal watering rate $Q_{opti}$ determined with the piecewise regression, and expected optimal rate neglecting sensible cooling, for all pavements.

| Pavement structure | $\Phi_{opti}$ (W/m²) | Segment 1 | Segment 2 | $Q_{opti}$ (mm/h) | $\langle\Phi_{reg,\ lat}\rangle/630$ (mm/h) |
|---|---|---|---|---|---|
| Asphalt road | 470 | $y_1 = 591\ Q$ | $y_2 = 24.5\ Q + 455$ | 0.80 | 0.80 |
| Asphalt sidewalk | 445 | $y_1 = 585\ Q$ | $y_2 = 14.2\ Q + 432$ | 0.76 | 0.72 |
| Stabilized sand | 290 | $y_1 = 555\ Q$ | $y_2 = 26.7\ Q + 281$ | 0.53 | 0.54 |
| Granite sidewalk | 375 | $y_1 = 543\ Q$ | $y_2 = 28.0\ Q + 355$ | 0.69 | 0.66 |
| Cobblestones | 345 | $y_1 = 528\ Q$ | $y_2 = 27.5\ Q + 327$ | 0.65 | 0.61 |
| Thermochromic asphalt | 380 | $y_1 = 647\ Q$ | $y_2 = 9.80\ Q + 377$ | 0.59 | 0.63 |
| NIR reflective asphalt | 270 | $y_1 = 534\ Q$ | $y_2 = 6.41\ Q + 270$ | 0.51 | 0.46 |
| Slag concrete sidewalk | 280 | $y_1 = 542\ Q$ | $y_2 = 7.94\ Q + 278$ | 0.52 | 0.47 |
| Permeable sidewalk 1 (w/o clay) | 350 | $y_1 = 527\ Q$ | $y_2 = 39.9\ Q + 326$ | 0.67 | 0.66 |
| Permeable sidewalk 2 (w/ clay) | 355 | $y_1 = 479\ Q$ | $y_2 = 25.2\ Q + 338$ | 0.74 | 0.63 |
| Pervious asphalt road | 380 | $y_1 = 506\ Q$ | $y_2 = 28.5\ Q + 360$ | 0.75 | 0.69 |

As mentioned in section 2.4, theoretically, the 1st segment's slope (latent regime) should be close to 630 W/m² per mm/h (corresponding to $l$ the latent heat of vaporization of water), given that sensible cooling is marginal. The corresponding slopes in Table 6 are globally lower than this, because of certain assumptions made for the calculation of $\Phi$, impacting the latent regime's slope. In particular, both the albedo and the emissivity are considered to be that of a wet sample as soon as watering is implemented, when strictly, they should be weighted by the time span during which the surface is completely dried out during the day phase. Also, the maximum surface temperature is used for the calculations when it would be preferable to consider an average temperature instead. Both these aspects should slightly affect the first regime. No difference would be observed for the largest watering rates, since the surface has no time to dry out (surface peaks disappear).

In addition, the latent regime's slope is also influenced by the specific surface of the sample (shape, flatness, porosity, etc.). Pervious structures are expected to have a lower slope for the first regime, as they infiltrate water at depth. Thus, qualitatively, the ratio of the latent regime's slope to the theoretical slope (i.e. $l$) allows to estimate the perviousness of the sample, while it gives us the relative accuracy of this estimation with impervious samples. For PPCC sidewalks and pervious asphalt, this ratio ranges from a porosity of ~15 to 25%. This ratio ranges between 5 to 10% for highly impervious structures (asphalt road sidewalk, granite), giving us the typical accuracy of the estimation.

In Table 6, as mentioned in section 4.1, brighter and thus cooler structures exhibit lower optimal watering rates $Q_{opti}$. Overall, this is better verified than for Table 5. The most significant difference concerns the PPCC sidewalks, for which much lower optimal watering rates are obtained using $\Phi$ instead of surface temperature variation (~0.7 mm/h against 0.9 mm/h respectively). We assume this is because the calculation of $\Phi$ relies on in-depth signals (via $\Delta V_0^{dry\text{-}wet}$) which dampens surface signal fluctuations (caused by convection, insolation, water sprinkling, etc.) and thus mitigates the effects of water infiltration that caused $Q_{opti}$ to increase with regard to impervious pavements. Furthermore, no significant difference in behaviour other than water infiltration is observed between PPCC 1 and 2, or between the pervious asphalt and the asphalt road, as runoff is inhibited in the chamber. As a result, impervious structures retain all of the sprinkled water at the surface, contrary to what would be observed in the field. This is further discussed in sections 6 and 7.

Table 6's last column lists the expected optimal watering rates neglecting sensible cooling (see section 2.4). The latter are estimated by intersecting the theoretical latent regime's slope, i.e. the cooling flux created by evaporating 1 mm of water per hour (630 W/m² per mm/h) ($y_1 = 630\ Q$), with the 2nd regime (sensible regime) zero-slope segment whose intercept is the maximum cooling flux reached on average for the last greatest rates ($y_2 = lE^{max} = \langle\Phi_{reg,\ lat}\rangle$). The optimal rate is thus given by the ratio $\langle\Phi_{reg,\ lat}\rangle/630$, in mm/h.

This method is found to be in good agreement with the values from the double piecewise regression, despite the first slope being underestimated, with residues less than 0.05 mm/h (apart from PPCC 2) which is within the typical accuracy of the watering rate calibration. This result indicates that a satisfying estimation of $Q_{opti}$ can be obtained in the lab with only one highly-watered test instead of a complete range of tests, provided

that enough information is known to fully estimate the corresponding pavement cooling flux and that sensible flux remains negligible.

Optimal watering rates versus albedo and absorptivity are plotted in Figure 14.

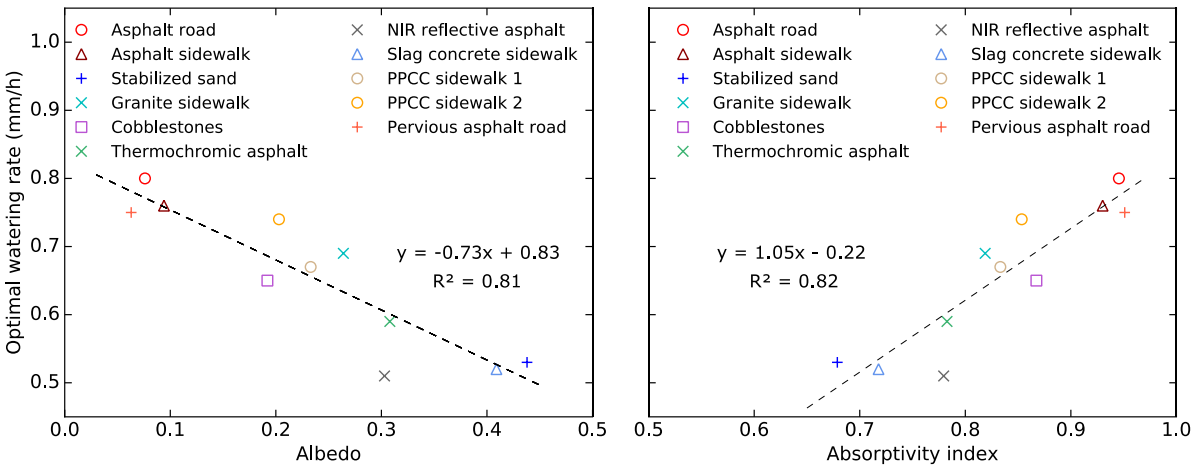


Figure 14: Optimal watering rate for each pavement structure as a function of their albedo (left) and their absorptivity (right).

Good linear agreement is found between $\mathcal{Q}_{opti}$ and the x-axis. Under the lab conditions, this figure infers that the theoretical maximum optimal watering rate would be around 0.83 mm/h for a conceptual surface with a null albedo, while the minimum would be 0.10 mm/h for a surface with an albedo of 1. Under known experimental conditions, such graph is useful to predict the amount of water a material would need to maximise the effects of pavement-watering only knowing its albedo and absorptivity. Good linear agreement is also found between $\mathcal{Q}_{opti}$ (mm/h) and dry daily absorbed radiation (kWh/m²), with $y = 0.13x + 0.11$ and $R^2 = 0.79$. Such cumulative daytime absorbed radiation for dry trials are summarized in the next section, in Table 7. This is unsurprising insofar as net radiation can be expressed as a function of the absorptivity index, and since surface temperature strongly depends on the albedo, a predominant term in the expression of the absorptivity $a$. This should be taken into account in the field and is discussed in section 6.

# 5 Steady-state thermal analysis

## 5.1 Surface partitioning of incident irradiance

We now compare how dry and optimally-watered pavements partition incident irradiance between convection, conduction, upward radiation and cooling flux. The heat budget of a pavement is expressed as:

$$S + L = S_{up} + L_{up} + H + V_0 + \Phi \tag{14}$$

Hence:

$$a(S + L) - \sigma\varepsilon T_s^4 = R_n = H + V_0 + \Phi \tag{15}$$

Energy partitioning helps understand the potential impact of pavements on pedestrian's heat budget. For instance, while radiosity $S_{up}+L_{up}$ helps to limit surface heating, it is detrimental to a pedestrian's radiative budget. Heat conduction on the other hand has no significant impact on pedestrians, while convective exchanges, in the absence of wind (low $h$) or advection, typical of heat-wave conditions, should be minimized in order to reduce atmospheric heating and heat stress as much as possible. Indeed, sensible heat release from a pavement, whether during day or night time, is identified as a major contributing factor to the warming of the near-surface air (Asaeda *et al.* 1996).

Figure 15 illustrates the heat flux to irradiance ratio for convective exchanges $H$, upward radiosity $S_{up}+L_{up}$, heat conduction $V_0$ and total cooling flux $\Phi$ as a function of the absorptivity index $a$ (eq. (13)) in steady-state. Dry trials and trials closest to the optimal watering rates $\mathcal{Q}_{opti}$ (Table 6) are represented. Note that for optimally-watered trials, the wet albedo and wet emissivity values are used for the calculation of $a$. For each dataset, the best linear regression is plotted with its equation and coefficient of determination $R^2$. Typical propagated uncertainties for $H$, $V_0$, and $S_{up}+L_{up}$ are about 10-20 W/m², i.e. a few percent of $S+L$, and about 20-30 W/m² for $\Phi$.

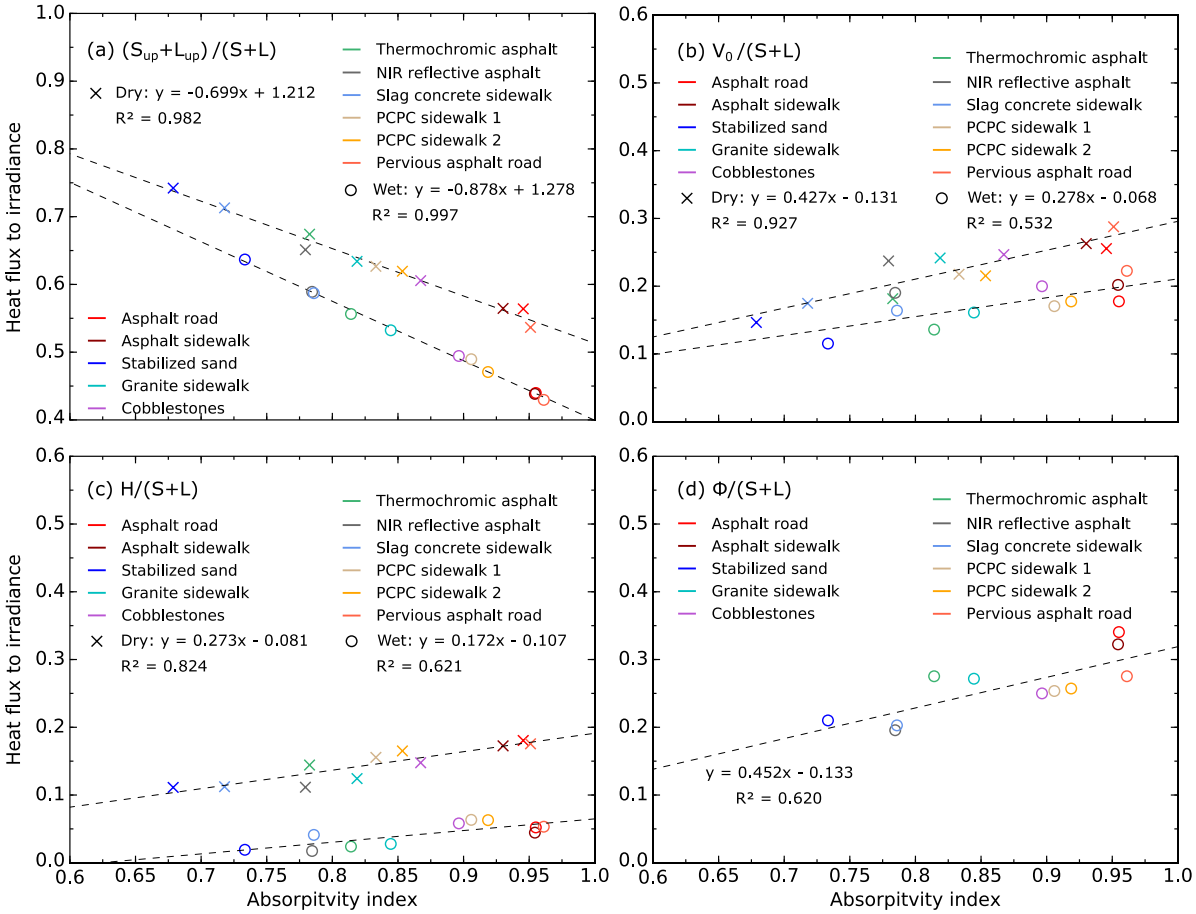


Figure 15: Steady-state surface partitioning of irradiance: (a): radiosity $S_{up}+L_{up}$, (b): conduction heat flux $V_0$, (c): atmospheric convective heat flux $H$ and (d): cooling flux $\Phi$, all divided by irradiance $S+L$ and plotted as a function of the absorptivity index $a$ for all pavements. Non-watered trials are represented with cross markers while optimally-watered trials with circle markers.

Figure 15 confirms previous observations and analyses. For all subfigures (a), (b), (c) and (d), the data plotted as a function of absorptivity exhibits a linear trend. This is directly inherited from equation (15) above, which in essence states that highly absorbing pavements will have high net radiation, and thus high $H$ and $V_0$ as a consequence, all else being equal. Qin & Hiller (2014) found a similar result for the daily cumulative energy flux, which decreased linearly with reflectivity. We start by describing the dry behaviour of the pavements.

In Figure 15 (a), materials with high absorptivity (low albedo and high emissivity) are found to absorb a large quantity of energy (lower radiosity $S_{up}+L_{up}$). Radiosity is as low as 56% of incident irradiance for the darkest structures while the dry pavement with the highest radiosity is the stabilized sand, closely followed by slag concrete, with resp. ratios of 74% and 71%.

For the darkest pavements, black-body emission is predominant in radiosity, as $S_{up}$ is low due to their small albedo. The contrary applies to the brightest pavements. As an example, the black-body emission of the asphalt road represents 51% of $S+L$ for a total radiosity of 56%, while it is 42% for the stabilized sand, which has a total radiosity of 74% of $S+L$. For comparison, daily absorbed radiation is listed in Table 7. Finally, the reflected LW is negligible for all structures (since (1-ε) is close to zero, and LW only account for 30% of the irradiance).

Among the remaining absorbed energy ($R_n$), a portion is transmitted in-depth by conduction $V_0$ and the other is released via $H$, convection to the atmosphere (eq. (2)).

In Figure 15 (b), partitioning of incident irradiance to conduction $V_0$ ranges from 15% to 26% for pavements with the lowest to the highest absorptivity, that is respectively stabilized sand to asphalt pavements. The same tendencies are obtained for convection $H$ (Figure 15 (c)), although smaller fractions of irradiance are involved. The latter ranges from 11% (stabilized sand) to 18% of $S+L$ at most (asphalt road). Discrepancies in the convective behaviour between pavements are thus significantly smoothed out.

Finally, other pavements have an intermediate behaviour, while reflective paints significantly reduce each term compared to unpainted asphalt sidewalk.

We now continue the analysis of Figure 15 with the data from the optimally-watered trials (depicted with circle markers).

In all cases, solar absorptivity increases with watering compared to a dry test, especially since albedo decreases with surface moistening. When the surface of a pavement is watered, the resulting cooling flux causes a reduction of convection and conduction, as well as a reduction of reflected and re-emitted radiation, resulting in an increase in net radiation. In other words, $\Phi$ is partitioned into reductions of $H$, $V_0$ and increase of $R_n$ (eq. (5)).

As can be seen in Figure 15 (d), a large proportion of irradiance is used to generate the cooling flux $\Phi$. This ranges from ~22% to 35% of $S+L$, pavement-watering being more efficient on materials with a higher absorptivity index. As a consequence, each term involved in the surface heat budget is strongly reduced by watering: radiosity drops between 42% and 64% of incident irradiance, conduction between 12% and 18% and convection between 2% and 5% of irradiance. Good agreement between $\Phi$ and $a$ also indicates the lower importance of the materials' thermo-physical properties in the efficiency of watering, the latter remaining relatively similar between samples.

Similar observations, regarding the proportions of convective exchanges and heat conduction as well as the strong impact of watering on $H$ were made by Takebayashi & Moriyama (2012) on asphalt and concrete pavements, whereas Qin & Hiller (2014) found a greater proportion of sensible heat $H$ with regard to heat conduction.

## 5.2 Surface partitioning of net radiation

Figure 16 shows the surface partitioning of net radiation for dry and optimally-watered trials. It provides information about the heat transfer mode favoured by each structure for transmitting the absorbed net radiation.

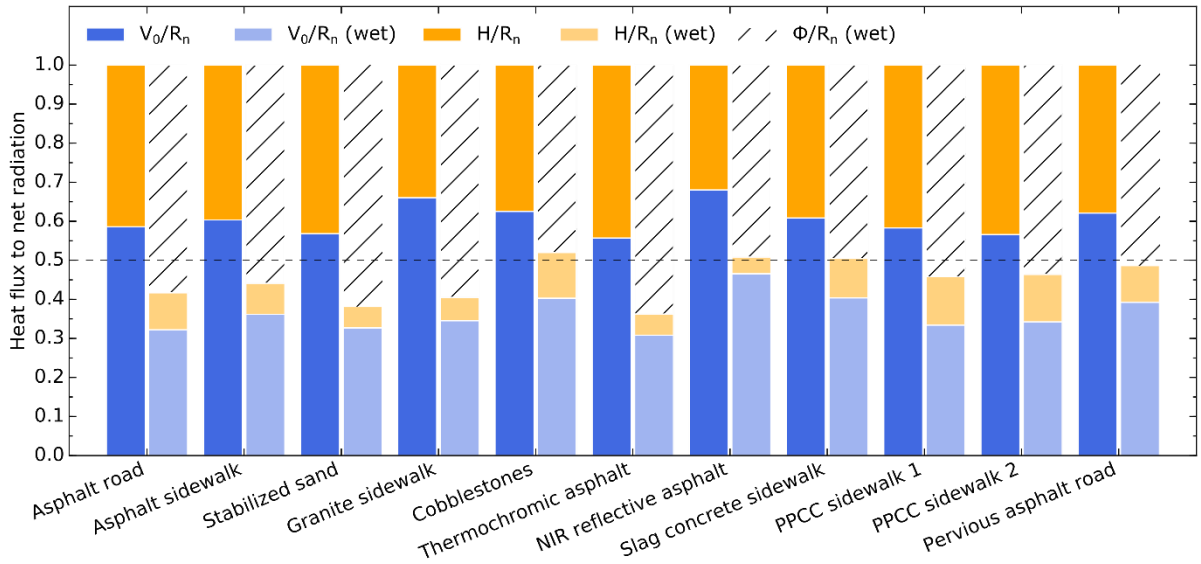


Figure 16: Steady-state net radiation surface partitioning for dry (left columns) and optimally-watered trials (right columns).

We begin by discussing results for dry trials. All structures exhibit a preference for conduction ($V_0/R_n$ partitioning > 0.5). Globally, it seems that the structures with the most conductive surface layer are those with the highest proportion of conduction. In order of decreasing apparent surface-layer conductivity: granite sidewalk, pervious and standard asphalt roads, cobblestones, PPCC sidewalk, asphalt sidewalk, stabilized sand and slag concrete sidewalk (see Table 4). Yet, the PPCC sidewalks exhibits a lower proportion of conduction to net radiation than the asphalt sidewalk, though the apparent conductivity of the upper layer is slightly higher. The same goes for the slag concrete sidewalk compared to stabilized sand. We assume this could be due to the imprecise estimation of $k$ due to steady state conditions not being fully reached and/or thermal leakage. In addition, the asphalt sidewalk, thermochromic and NIR reflective asphalts being the same structure, the value of $V_0/R_n$ should remain unchanged, since only the surface radiative properties

($\alpha$, $\varepsilon$) are modified. This lends credibility to the hypothesis that the albedo of thermochromic asphalt is slightly overestimated (see section 3.1).

These intrinsic behaviours are not altered by watering. Both $V_0$ and $H$ are strongly reduced by watering, although convective exchanges are further reduced in proportion.

A recap of all steady-state heat-fluxes as well as the cumulative absorbed daytime radiation for dry pavements is provided in Table 7. Summing errors may occur due to rounding, while $\Phi$ may slightly differ from Table 6 for which values are obtained directly from the piecewise regression, whereas values of Table 7 are calculated as residuals of the heat budget.

Table 7: Cumulative absorbed daytime radiation of dry pavements ($\int^{day} R_n\, dt$, in kWh/m²), and detailed steady-state heat budgets for dry and optimally-watered pavements (in W/m²).

| Pavement structure | Dry pavement | | | | | | Optimally-watered pavement | | | | | |
|---|---|---|---|---|---|---|---|---|---|---|---|---|
| | $\int^{day} R_n\, dt$ | $R_n$ | $V_0$ | $H$ | $S_{up}$ | $L_{up}$ | $R_n$ | $V_0$ | $H$ | $S_{up}$ | $L_{up}$ | $\Phi$ |
| Asphalt road | 5.4 | 601 | 351 | 250 | 71 | 708 | 773 | 245 | 72 | 53 | 554 | 456 |
| Asphalt sidewalk | 5.2 | 598 | 360 | 238 | 87 | 695 | 775 | 279 | 61 | 54 | 551 | 435 |
| Stabilized sand | 3.1 | 357 | 203 | 154 | 407 | 616 | 501 | 159 | 26 | 359 | 520 | 316 |
| Granite sidewalk | 4.3 | 505 | 333 | 172 | 246 | 629 | 645 | 222 | 38 | 206 | 529 | 385 |
| Cobblestones | 4.5 | 543 | 340 | 204 | 179 | 658 | 698 | 276 | 80 | 134 | 548 | 342 |
| Thermochromic asphalt | 3.9 | 450 | 250 | 200 | 286 | 644 | 612 | 188 | 33 | 247 | 521 | 391 |
| NIR reflective asphalt | 4.1 | 482 | 328 | 154 | 282 | 616 | 567 | 275 | 25 | 288 | 525 | 267 |
| Slag concrete sidewalk | 3.3 | 397 | 241 | 155 | 380 | 603 | 570 | 226 | 57 | 286 | 524 | 287 |
| Pervious sidewalk 1 (w/o clay) | 4.4 | 513 | 300 | 215 | 217 | 650 | 704 | 235 | 88 | 121 | 555 | 381 |
| Pervious sidewalk 2 (w/ clay) | 4.4 | 534 | 306 | 228 | 189 | 657 | 730 | 245 | 87 | 103 | 547 | 398 |
| Pervious asphalt road | 5.2 | 639 | 397 | 242 | 59 | 682 | 787 | 307 | 74 | 45 | 548 | 406 |

## 5.3 In-depth heat transmission

Having considered surface cooling efficiency, we now end the results section with heat transmission in-depth. We propose a dimensionless solar transmission index derived from Hendel *et al.* (2018), denoted $\tau$, that takes into account the composite structure of the pavements to better understand their behaviour in-depth. The index $\tau$ depends on depth $z$ through the thickness of the $i$-th composite layer $e_i$ and its corresponding apparent conductivity $k_i$, and also on the solar absorptivity index $a$ define formerly. The transmission index is the following:

$$\tau(z<0) = a.\frac{{e_0}/{k_0}}{\sum_i {e_i}/{k_i}} \tag{16}$$

The term $\frac{1}{\sum_i {e_i}/{k_i}}$ is the composite apparent thermal conductance of the overlaying material layers (in W/(m².K)). The numerator term ${e_0}/{k_0}$ is taken as a reference thermal resistance equal to 1 K.m²/W to render $\tau$ dimensionless. Figure 17 illustrates the ratio of in-depth heat flux to irradiance $S+L$ as a function of the transmission index $\tau$. Although heat conduction in-depth has no major impact on a pedestrian's heat budget during the day, it contributes to air temperature increase at night during pavement heat release.

As can be seen, good correlation is found with the proposed index. In Figure 17 (a), the granite sidewalk, although much more reflective than bituminous pavements, transmits as much heat 6 cm deep due to its high thermal conductivity. Similarly, cobblestones transmit as much 11 cm deep as the asphalt road 14 cm. In-depth, cobblestones are expected to exhibit a behaviour close to that of granite. However, cobblestones' apparent thermal conductivity is lower that granite's due to the composite nature of the sample. Conclusions are rendered even more difficult because of the different instrumentation of the samples (6 or 14 cm deep for granite against -11 cm for cobblestones).

The use of reflective paints on the asphalt sidewalk significantly reduces heat transmitted in-depth. Reflective asphalt thus transmits as little heat 6 cm deep as traditional asphalt does 14 cm deep. As expected, slag concrete is the structure transmitting the least heat both 6 cm and 14 cm deep, due to the combination of its low thermal conductivity and low absorptivity.

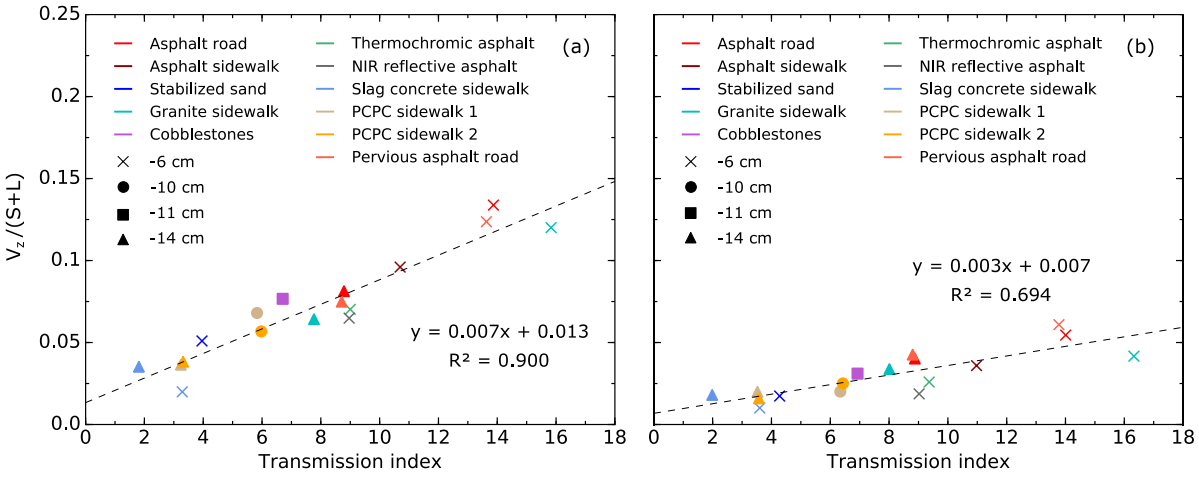


Figure 17: Steady-state heat fluxes in-depth (at 6, 10, 11 and 14 cm deep) to irradiance as a function of the transmission index for all pavements during a dry trial (a) and an optimally-watered trial (b).

Figure 17 (b) shows that optimal watering does not modify the previous trends, but significantly reduces the amount of transmitted heat.

Although high-inertia pavements may dampen the temperature increase during the day, this reduction is only limited to a few degrees (Qin & Hiller 2014), and accumulated heat remains a disadvantage at night and contributes to extend heat-waves. In such a case, heat-harvesting pavements (with heat exchangers for domestic hot water supply for example) can help limit heat release at night without prejudicing people during the day by decreasing surface temperature as well (Yinfei *et al.* 2018, Shaopeng *et al.* 2011, Chen *et al.* 2011). Depending on the purpose, in order to limit heat release at night, the use of relatively low heat-conducting pavements can be preferable. Nevertheless, such pavements tend to increase surface temperature increase during the day, detrimental for pedestrians when they are most exposed (Yinfei *et al.* 2014). Thus, they must be correlated with low surface temperature during the day (high albedo, shading, etc.).

# 6 Transferability to the field

Although the results presented in this paper here are not adapted to accurately describe field experiments, we now discuss the implications of transferring the optimal watering rates obtained in the lab to the field. It should be noted that this transposition is not straightforward, and is highly dependent on field parameters, particularly convection (e.g. the convective heat transfer coefficient $h$), conduction and net radiation, which are likely to increase or decrease optimal watering rates.

Comparison of the lab results for the asphalt road to a given field experiment for a similar structure showed that surface heat budget is roughly doubled (for conduction, convection and evaporative flux). Indeed, during daytime, the lab structure absorbs about twice as much net solar radiation as in the field (Hendel *et al.* 2015, Parison *et al.* 2020b). In addition, in the lab, good agreement is found between the optimal watering rate and the absorptivity index, as well as with daily absorbed net radiation (see section 4.3). This is used as a naïve approach for transposing results to the field for other pavements. Conditions inside the climate chamber requires about twice as much water to be sprinkled to reach the optimal rate for a given structure with regard to what would *a priori* be observed in the field, all else being equal (Parison *et al.* 2020b).

Yet, field experimentation poses strong technical and operational constraints, setting the limits of this approach. For instance, several factors are not reproduced in the laboratory, such as the curvature of the Haussmannian roads that causes water to run off to the drainage system via the gutters. Therefore, under real conditions, it is essential to take into account the surface water retention capacity of the pavement to modulate the frequency between two consecutive waterings in order to sprinkle the structure with the optimal rate, adapted to the quantity of water it is able to retain (which is about its surface roughness). For example, an optimal rate of 0.4 mm/h for the asphalt road (0.8 mm/h in the chamber) with a surface retention capacity of 0.2 mm requires watering every half hour. Thus, by adjusting the frequency between each cycle, the optimal watering rate can be achieved. For pervious materials however, since the optimal watering rate is *a priori* lower than the water retention capacity of the structure, unlike impervious structures,

more freedom on the frequency is given, for example by saturating the structure with water and re-water it only once it has evaporated entirely.

In this respect, the question of the infrastructure dedicated to pavement-watering is crucial. Previous field experiments were carried out in Paris using cleaning trucks and Paris' non-potable water network, which brought up many constraints (noise and visual nuisances, discomfort for the workers, heavy traffic, etc.), the strongest of which being the incompressibility of the minimum time span between two consecutive watering cycles and the lack of fine control over the quantity of water sprinkled, due to the fixed volume of the water tank and the operating pressure of the cleaning truck. Important re-filling time spans at the devoted non-potable water outlets also proved to be a problem. These aspects compromise the technical feasibility of the method.

In the future, if pavement-watering were to be deployed on a permanent basis as an emergency cooling tool applied to specific pre-identified relevant areas, an automated sprinkling device should be considered, as it has already been done it other cities (Yamagata *et al.* 2008, Takahashi *et al.* 2010). The device could be connected to the non-potable water network or re-use collected rainwater.

# 7 Conclusion

A lab experiment was used to study the thermal behaviour of six standard pavements commonly found in the Parisian urban fabric (asphalt road, asphalt sidewalk, granite sidewalk, stabilized sand, cobblestones and grass), as well as six innovative pavements (thermochromic and near-infrared reflective asphalt, slag concrete, two formulations of pervious concretes and a pervious asphalt road). Structures were constructed with the same composition as in the field. The experiment reproduces conditions similar to those observed during a heat wave in Paris, with an 8h heat-up phase with artificial insolation followed by a 16h night phase, thus allowing the comparison of each pavement under given conditions without having to implement long-lasting and costly fields tests. Surface and in-depth measurements are used to study the dry or watered behaviour of the samples, with more than ten different watering rates carried out in order to fine-tune the process before deployment in the field.

The lowest surface temperature was observed for the slag concrete structure, while dry grass was quite hot in the absence of evapotranspiration. Reflective paints allowed the asphalt sidewalk surface temperature to be reduced up to 6°-9°C. Such solutions are of particular interest for urban planners as they remain relatively cheap and easy to implement.

The surface heat budget was evaluated under steady-state conditions to determine the cooling flux as well as the reductions in heat conduction and convective exchanges and the increase in net radiation due to watering. Results are consistent with pavement-watering field campaigns in Paris were observed when factoring in the stronger incident irradiance in the lab (Parison *et al.* 2020b). The intersection of two cooling flux regimes versus the watering rate was used to determine the optimal rate, namely that equal to the evaporation rate for a given structure given the experimental conditions. Results also confirmed that a satisfactory estimate of the optimal watering rates could be easily achieved by performing only one highly-watered test instead of a wide range of trials, requiring the assessment of the corresponding cooling flux and the neglecting of sensible cooling flux. Optimal watering rates show a good correlation with the surface absorptivity index. This information can be used to predict the optimal amount of water to spray on a given surface.

Finally, the partitioning of irradiance and net radiation into atmospheric, ground, upwards and evaporative heat fluxes was studied versus the absorptivity, for dry and optimally-watered pavements. Results show that bituminous structures, i.e. those with the highest absorptivity, are the most detrimental in all regards, while stabilized sand and slag concrete, both fairly insulating and reflective, are the most favourable. From the most to the least favourable pavements respectively, irradiance surface partitioning is split into 1,020-770 W/m² of radiosity, 210-360 W/m² of conduction and 150-250 W/m² of convection. Watering significantly reduces each term, respectively dropping to 580-880 W/m² for radiosity, 165-250 W/m² for conduction and as low as 30-70 W/m² for convection.

In the end, sensible atmospheric convection is significantly and efficiently reduced, hopefully for limiting the heating up of air negatively impacting pedestrians. Total optimal cooling ranges from 300-480 W/m², and is correlated as well with the absorptivity index. This means that the technique is more effective with highly absorptive materials.

In-depth, the transmitted heat flux correlates linearly with a transmission index taking into account the absorptivity and apparent conductivity of the material layers. The most conductive structures (such as granite) tend to conduct as much heat in-depth as the darkest structures, even if they are less absorbing.

Future work mainly concerns the improvement of the experimental protocol. The latter proved ill-suited for the study of the influence of a material's permeability other than by showing water infiltration at the surface due to the lack of runoff inside the chamber, and to the chosen watering protocol (fixed amount of sprinkled water with varying frequencies). Contrariwise, in the field, pervious sub-layers permit lowering the frequency while runoff make it necessary to water an impervious pavement more frequently, for a given evaporation rate and quantity of water sprinkled.

Although the setpoint values imposed for the day and night phases were selected to be representative of a Parisian heat wave, they remain relatively far from realistic conditions. This leaves room for improvement, for example by imposing dynamic ramps of temperature, relative humidity and artificial insolation rather than fixed values. This would also allow the study of the samples in transient state, which would be much more realistic and would allow for the study of the pavements' thermal inertia. The use of lamps with a spectrum closer to that of the sun is also considered, as halogen lamps are shifted in the infrared band, which mostly plays a role on the albedos of the pavements. For instance, the NIR reflective paint's albedo is 11% less considering the solar spectrum, and is thus expected to be less favourable under real conditions. Also, although a wide range of pavements were studied, no highly reflective structures were tested. Such pavements should be looked at in the future in order to validate the possible existence of radiative cooling in the chamber. Regardless of how many improvements are implemented, a lab experiment will never capture the full reality of field conditions and can only provide simplified pavement behaviours. On the other hand, more flexibility is available for instrumentation of the samples than in the field.

On a broader perspective, preferably, the combination of different cooling techniques should be favoured for an increased efficiency. Solutions adapted to the type of location (square, sidewalk, etc.), its characteristics (daily insolation, street orientation, pedestrian traffic, vulnerability of local inhabitants, existing pavement materials, etc.), the people targeted (pedestrians or others) and the hour of the day (morning, afternoon, etc.), must be deployed in order to properly cool the population.

To tackle this aspect, a GIS tool can be used to identify priority areas in terms of population exposure and vulnerability, foreseeing their redesigning into cooler areas. Such tool aims to propose cooling solutions adapted to the sites identified depending on their cooling potential (Hendel *et al.* 2019). On this basis, other simple cooling solutions may be proposed, such as sun-shading or vegetation. Generally speaking, solutions targeting buildings (solar exposition, ventilation and insulation) should also be considered in order to fully protect the population.

Finally, although low pavement surface temperatures should help reduce air temperature in urban areas, the precise effect on the urban canopy layer as well as pedestrians' thermal stress, surrounding building etc. remains poorly known (Qin 2015). Knowledge in this area will need to be refined in future research, and in this regard, further comparison of the lab results with additional field tests would also be useful. Such tests would also test the durability (over time and in terms of resistance to dirt) of paints, and should be completed with microclimatic measurements to estimate the exact effective gain on pedestrian's heat stress.

Other aspects can also be considered as a cooling solution selection criteria ($CO_2$ emission during pavements manufacture, positive or negative impact on the biodiversity of the pavements, water restriction measures etc.). In this respect, synergies with other urban planning projects are interesting, such as the use of pervious materials for the collection and reuse of rainwater (whether for pavement-watering or not). In addition to reducing the frequency of watering for a given rate, such materials are also useful for stormwater management.

# Acknowledgments

Funding for this study was provided by the Paris City Hall. The authors acknowledge the significant support of the Roads and Traffic and the Waste and Water Divisions for their technical assistance, time and expertise. The authors would also like to thank Mr. H. Leuck at *MCI Technologie* for helping with the realization of the thermochromic paint samples.

# References


Anandakumar, K. (1999). A study on the partition of net radiation into heat fluxes on a dry asphalt surface. *Atmospheric Environment*, *33*(24-25), 3911-3918.

Asaeda, T., Ca, V. T., & Wake, A. (1996). Heat storage of pavement and its effect on the lower atmosphere. *Atmospheric environment*, *30*(3), 413-427.

ASTM. (2012). Standard test method for solar absorptance, reflectance, and transmittance of materials using integrating spheres.

Azam, M. H., Bernard, J., Morille, B., Musy, M., & Andrieu, H. (2018). A pavement-watering thermal model for SOLENE-microclimat: development and evaluation. *Urban Climate*, *25*, 22-36.

Bowler, D. E., Buyung-Ali, L., Knight, T. M., & Pullin, A. S. (2010). Urban greening to cool towns and cities: A systematic review of the empirical evidence. *Landscape and urban planning*, *97*(3), 147-155.

Camuffo, D., & Bernardi, A. (1982). An observational study of heat fluxes and their relationships with net radiation. *Boundary-Layer Meteorology*, *23*(3), 359-368.

Chen, B. L., Bhowmick, S., & Mallick, R. B. (2009). A laboratory study on reduction of the heat island effect of asphalt pavements. *Journal of the Association of Asphalt Paving Technologists*, *78*, 209-248.

Daniel, M., Lemonsu, A., & Viguie, V. (2018). Role of watering practices in large-scale urban planning strategies to face the heat-wave risk in future climate. *Urban Climate*, *23*, 287-308.

De Munck, C., Pigeon, G., Masson, V., Meunier, F., Bousquet, P., Tréméac, B., ... & Marchadier, C. (2013). How much can air conditioning increase air temperatures for a city like Paris, France?. *International Journal of Climatology*, *33*(1), 210-227.

De Munck, C., Lemonsu, A., Masson, V., Le Bras, J., & Bonhomme, M. (2018). Evaluating the impacts of greening scenarios on thermal comfort and energy and water consumptions for adapting Paris city to climate change. *Urban Climate*, *23*, 260-286.

Dousset, B., Gourmelon, F., Laaidi, K., Zeghnoun, A., Giraudet, E., Bretin, P., ... & Vandentorren, S. (2011). Satellite monitoring of summer heat waves in the Paris metropolitan area. *International Journal of Climatology*, *31*(2), 313-323.

Guo, X., & Hendel, M. (2018). Urban water networks as an alternative source for district heating and emergency heat-wave cooling. *Energy*, *145*, 79-87.

Hanna, E., & Tait, P. (2015). Limitations to thermoregulation and acclimatization challenge human adaptation to global warming. *International journal of environmental research and public health*, *12*(7), 8034-8074.

Hendel, M., Colombert, M., Diab, Y., & Royon, L. (2015). An analysis of pavement heat flux to optimize the water efficiency of a pavement-watering method. *Applied thermal engineering*, *78*, 658-669.

Hendel, M., Gutierrez, P., Colombert, M., Diab, Y., & Royon, L. (2016). Measuring the effects of urban heat island mitigation techniques in the field: Application to the case of pavement-watering in Paris. *Urban Climate*, *16*, 43-58.

Hendel, M., Parison, S., Grados, A., & Royon, L. (2018). Which pavement structures are best suited to limiting the UHI effect? A laboratory-scale study of Parisian pavement structures. *Building and Environment*, *144*, 216-229.

Hendel, M., Bobée, C., Karam, G., Parison, S., Berthe, A., Bordin, P., & Royon, L. (2019). Developing a GIS Tool for Emergency Urban Cooling in Case of Heat-Waves. *Urban Climate*, (under review).

Kang, S., & Eltahir, E. A. (2018). North China Plain threatened by deadly heatwaves due to climate change and irrigation. *Nature communications*, *9*(1), 2894.

Karlessi, T., Santamouris, M., Apostolakis, K., Synnefa, A., & Livada, I. (2009). Development and testing of thermochromic coatings for buildings and urban structures. *Solar Energy*, *83*(4), 538-551.

Kinouchi, T., & Kanda, M. (1997). An Observation on the Climatic Effect of Watering on Paved Roads. *Journal of Hydroscience and Hydraulic Engineering*, *15*(1), 55–64.

Lemonsu, A., Kounkou-Arnaud, R., Desplat, J., Salagnac, J. L., & Masson, V. (2013). Evolution of the Parisian urban climate under a global changing climate. *Climatic change*, *116*(3-4), 679-692.

Levinson, R., Akbari, H., & Reilly, J. C. (2007). Cooler tile-roofed buildings with near-infrared-reflective non-white coatings. *Building and Environment*, *42*(7), 2591-2605.

Li, H., Harvey, J., & Kendall, A. (2013a). Field measurement of albedo for different land cover materials and effects on thermal performance. *Building and environment*, *59*, 536-546.

Li, H., Harvey, J. T., Holland, T. J., & Kayhanian, M. (2013b). Corrigendum: The use of reflective and permeable pavements as a potential practice for heat island mitigation and stormwater management. *Environ. Res. Lett*, *8*(4), 049501.

Meehl, G. A., & Tebaldi, C. (2004). More intense, more frequent, and longer lasting heat waves in the 21st century. *Science*, *305*(5686), 994-997.

Mora, C., Dousset, B., Caldwell, I. R., Powell, F. E., Geronimo, R. C., Bielecki, C. R., ... & Lucas, M. P. (2017). Global risk of deadly heat. *Nature Climate Change*, *7*(7), 501.

Oke, T. R. (1988). The urban energy balance. Progress in Physical geography, 12(4), 471-508.

Oke, T. R. (1997). Urban environments. *The surface climates of Canada*, 303-327.

Parison, S., Hendel, M., Grados, A., Jurski, K., & Royon, L. (2019). A radiative technique for measuring the thermal properties of road and urban materials. Road Materials and Pavement Design, 1-15.

Parison, S., Hendel, M., & Royon, L. (2020a). An Updated Method for Quantifying the Field Effects of Urban Heat Island Mitigation Techniques. *Urban Climate,* (under review)

Parison, S., Hendel, M., Grados, A., Jurski, K., & Royon, L. (2020b). A lab experiment for optimizing the cooling efficiency and the watering rate of pavement-watering. *Urban Climate*, *31*, 100543.

Pomerantz, M. (2000). The effect of pavements' temperatures on air temperatures in large cities.

Pomerantz, M., Akbari, H., Chang, S. C., Levinson, R., & Pon, B. (2003). Examples of cooler reflective streets for urban heat-island mitigation: Portland cement concrete and chip seals (No. LBNL-49283). Lawrence Berkeley National Lab.(LBNL), Berkeley, CA (United States).

Qin, Y., & Hiller, J. E. (2014). Understanding pavement-surface energy balance and its implications on cool pavement development. *Energy and Buildings*, *85*, 389-399.

Qin, Y. (2015). A review on the development of cool pavements to mitigate urban heat island effect. *Renewable and sustainable energy reviews*, *52*, 445-459.

Robine, J. M., Cheung, S. L. K., Le Roy, S., Van Oyen, H., Griffiths, C., Michel, J. P., & Herrmann, F. R. (2008). Death toll exceeded 70,000 in Europe during the summer of 2003. *Comptes rendus biologies*, *331*(2), 171-178.

Santamouris, M. (2013). Using cool pavements as a mitigation strategy to fight urban heat island—A review of the actual developments. *Renewable and Sustainable Energy Reviews*, *26*, 224-240.

Santamouris, M. (2015). Regulating the damaged thermostat of the cities—Status, impacts and mitigation challenges. *Energy and Buildings*, *91*, 43-56.

Shaopeng, W., Mingyu, C., & Jizhe, Z. (2011). Laboratory investigation into thermal response of asphalt pavements as solar collector by application of small-scale slabs. *Applied Thermal Engineering*, *31*(10), 1582-1587.

Sherwood, S. C., & Huber, M. (2010). An adaptability limit to climate change due to heat stress. *Proceedings of the National Academy of Sciences*, *107*(21), 9552-9555.

Shin, D. U., Bae, W. B., Park, Y. M., Kim, S. R., & Kim, Y. G. (2019). Method for evaluating the heat-island mitigation effect of porous/water-retentive blocks using a climatic chamber. *Water Science and Technology*, *80*(5), 855-863.

Synnefa, A., Santamouris, M., & Apostolakis, K. (2007). On the development, optical properties and thermal performance of cool colored coatings for the urban environment. *Solar energy*, *81*(4), 488-497.

Takahashi, R., Asakura, A., Koike, K., Himeno, S., & Fujita, S. (2010). Using Snow Melting Pipes to Verify the Water Sprinkling's Effect over a Wide Area. In *NOVATECH 2010* (p. 10).

Takebayashi, H., & Moriyama, M. (2012). Study on surface heat budget of various pavements for urban heat island mitigation. *Advances in Materials Science and Engineering*, *2012*.

Tremeac, B., Bousquet, P., De Munck, C., Pigeon, G., Masson, V., Marchadier, C., ... & Meunier, F. (2012). Influence of air conditioning management on heat island in Paris air street temperatures. *Applied Energy*, *95*, 102-110.

Ueno, T., & Tamaoki, K. (2009). Thermal characteristics of urban land cover by indoor lamp-irradiation experiment. In *The Seventh International Conference on Urban Climate* (pp. 1-4).

Wu, H., Sun, B., Li, Z., & Yu, J. (2018). Characterizing thermal behaviors of various pavement materials and their thermal impacts on ambient environment. *Journal of cleaner production*, *172*, 1358-1367.

Xie, N., Li, H., Zhao, W., Zhang, C., Yang, B., Zhang, H., & Zhang, Y. (2019). Optical and durability performance of near-infrared reflective coatings for cool pavement: Laboratorial investigation. *Building and Environment*, *163*, 106334.

Yamagata, H., Nasu, M., Yoshizawa, M., Miyamoto, A., & Minamiyama, M. (2008). Heat island mitigation using water retentive pavement sprinkled with reclaimed wastewater. *Water science and technology*, *57*(5), 763-771.

Yinfei, D., Qin, S., & Shengyue, W. (2014). Highly oriented heat-induced structure of asphalt pavement for reducing pavement temperature. *Energy and Buildings*, *85*, 23-31.

Yinfei, D., Zheng, H., Jiaqi, C., & Weizheng, L. (2018). A novel strategy of inducing solar absorption and accelerating heat release for cooling asphalt pavement. *Solar Energy*, *159*, 125-133.